Nucleic Acids Research, 2026, **54**, gkag575
https://doi.org/10.1093/nar/gkag575
NAR Breakthrough Article

Antisense RNA controls the degradation of phycobilisomes in heterocyst-forming cyanobacteria by a transcriptional interference mechanism

Isidro Álvarez-Escribano [1,†], Manuel Brenes-Álvarez [2,†], Jens Georg [2], Agustín Vioque [1], Alicia M. Muro-Pastor [1,*]

[1]Instituto de Bioquímica Vegetal y Fotosíntesis, Consejo Superior de Investigaciones Científicas and Universidad de Sevilla, E-41092 Sevilla, Spain
[2]Genetics and Experimental Bioinformatics, Faculty of Biology, University of Freiburg, D-79104 Freiburg, Germany

*To whom correspondence should be addressed. Email: alicia@ibvf.csic.es
†The first two authors should be regarded as Joint First Authors.

Abstract

Transcriptional interference is rarely documented in bacteria. In cyanobacteria, phycobilisomes are the major light-harvesting antennae, and their degradation under non-optimal conditions follows a tightly regulated genetic program leading to the production of NblA, a widely conserved proteolytic adapter. NblA production is regulated at both the transcriptional and post-transcriptional levels. Here, we uncover an additional regulatory layer mediated by an antisense RNA conserved in heterocyst-forming cyanobacteria. In *Nostoc* sp. PCC 7120, transcription of the abundant antisense RNA (*as_nblA*) limits *nblA* mRNA accumulation. A strain unable to transcribe *as_nblA* produces an excess of NblA, ultimately so harmful that suppressor mutations of *nblA* expression accumulate rapidly, underscoring the essential role of *as_nblA*. Rifampicin time-series experiments and the inability of *as_nblA* to regulate *nblA* expression in *trans* support transcriptional interference as the primary regulatory mechanism of *as_nblA*. Mathematical modeling of *nblA* expression, supported by biological data, shows that *as_nblA* plays a pivotal role in preventing leaky *nblA* expression under non-inducing conditions. Our work highlights the importance of antisense RNA-mediated regulation, particularly transcriptional interference, in establishing thresholds that prevent spurious expression of genes encoding critical cellular functions.

Lay summary

Cyanobacteria need to carefully control how they respond to stress. This study shows how the expression of a gene (*nblA*) that triggers the breakdown of light-harvesting phycobilisomes is tightly regulated. We discovered that an antisense RNA prevents unwanted NblA production under non-stress conditions. When this control is removed, excess NblA damages phycobilisomes and slows growth. Experiments and modeling reveal that this regulation works mainly by interference with gene transcription. Another small RNA provides additional regulation. Together, these mechanisms ensure NblA is produced only when needed, such as during nutrient stress, helping cells adapt while avoiding harmful overreactions. Overall, the study highlights how antisense RNAs help cells avoid harmful gene activity while allowing rapid responses to environmental stress.

Graphical abstract

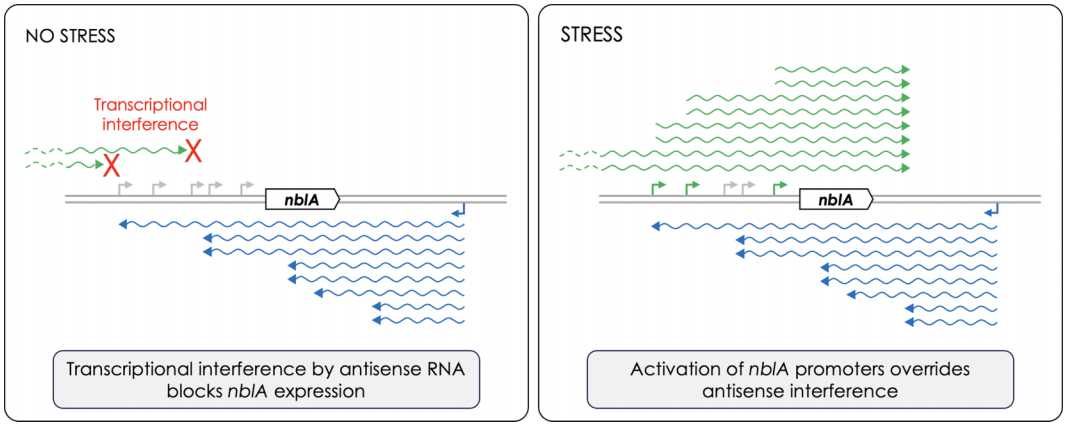

Received: March 27, 2026. **Revised:** May 12, 2026. **Accepted:** May 21, 2026

Introduction

The NblA protein plays a crucial role in the environmentally regulated degradation of the phycobilisomes (PBS), which are essential light-harvesting complexes that transfer light energy to the photosystems in cyanobacteria. Degradation of PBS (also referred to as bleaching) is particularly significant under nutrient-limiting conditions, such as nitrogen starvation. NblA was first described in the unicellular cyanobacterium *Synechococcus elongatus* PCC 7942 as a small polypeptide that triggered the degradation of phycobiliproteins (PBP) under nutritional limitation, with the expression of the *nblA* gene being induced upon nitrogen, sulfur, or phosphate removal [1]. Since PBS account for a large amount of the total protein content in the cells, and therefore a large amount of the total nitrogen content, bleaching under those circumstances is an adaptive strategy that allows the cyanobacteria to recycle nutrients under stress conditions. Induction of *nblA* transcription and PBS degradation have also been observed upon exposure to high light in *S. elongatus* PCC 7942 [2], preventing excessive energy input to the photosynthetic apparatus. NblA functions as a proteolysis adapter protein that interacts with PBP, facilitating their degradation by the Clp protease complex [3–6]. This interaction is critical, because it designates PBP for degradation, thereby allowing the cyanobacteria to recycle nutrients and adjust light absorbance to their metabolic capacity. Recently, *nblA* has emerged as a gene with a broad impact at the ecological level because the presence of active NblA proteins encoded in cyanophages negatively affects oceanic cyanobacterial photosynthesis [7].

In contrast to unicellular non-diazotrophic cyanobacteria, which usually nearly completely degrade PBP within 1–2 days of nitrogen deprivation, the PBS in vegetative cells of heterocyst-forming cyanobacteria, such as *Nostoc* sp. PCC 7120 (also known as *Anabaena* sp. PCC 7120, from now on, *Nostoc*), are only transiently degraded until the nitrogenase located in specialized cells, called heterocysts, becomes active and combined nitrogen forms are again available to support the growth of the filament. In these strains, which are ultimately able to fix atmospheric nitrogen, the transient response to combined nitrogen deficiency involves the induction of the *nblA* gene and partial degradation of PBS [4, 8]. However, PBS degradation proceeds near completion only in heterocysts, terminally differentiated cells where the photosynthetic apparatus is dismantled, and therefore the consequences of the *nblA* mutation in *Nostoc* are more obvious in this specialized cell type, as heterocysts of an *nblA* null mutant retain PBP [8]. The expression of *nblA* is induced upon nitrogen removal [9], and the accumulation of *nblA* transcripts is very low in a mutant of the major nitrogen homeostasis transcription factor gene *ntcA* [10]. In addition, post-transcriptional regulation by a small, nitrogen-regulated non-coding RNA (NsrR1, nitrogen stress-repressed RNA 1) has been described to inhibit the translation of the *nblA* transcript in *Nostoc* [10]. Overexpression of NsrR1 leads to degradation of the *nblA* transcript, suggesting reduced stability of the untranslated mRNA. Under nitrogen-replete conditions, the interaction of the *nblA* mRNA with NsrR1 was proposed to reduce translation of the small amounts of NblA protein resulting from leaky *nblA* transcription [10]. In the case of unicellular non-nitrogen fixing strains, the redox-responsive transcription factor RpaB has been described to regulate *nblA* expression in response to changes in light availability [2, 11].

Similar to the observations made for other groups of bacteria, transcriptomic analyses carried out in both unicellular and filamentous cyanobacteria have shown abundant transcription of antisense RNAs (asRNAs) [12]. In the case of *Nostoc*, early transcriptomic approaches already pointed to the relevance of antisense transcription [9, 13], and the recent definition of the transcriptomic map for this organism shows that in this heterocyst-forming cyanobacterium ~65% of the transcriptional units contain regions in antisense orientation to another transcriptional unit [14]. Physiological consequences of such antisense transcription are largely unexplored, but transcription of asRNAs may have regulatory consequences on the genes they overlap. In *Nostoc* post-transcriptional regulation operated by nitrogen-regulated asRNAs has been described for *glpX*, encoding sedoheptulose-1,7-bisphosphatase/fructose-1,6-bisphosphatase [15], *gltA*, encoding citrate synthase [14], and *glnA*, encoding glutamine synthetase [16]. In the case of *glpX* and *gltA*, the expression of their asRNAs specifically in heterocysts would contribute to the metabolic remodeling that takes place in this specific cell type, in particular affecting flows through the Calvin cycle and the tricarboxylic acid cycle, respectively.

The main regulatory mechanisms described for bacterial asRNAs are the co-degradation of the asRNA–mRNA duplexes and different types of transcriptional interference (TI) [17]. While several reports have described the co-degradation of asRNA–mRNA duplexes by RNase III in bacteria [18–20], including cyanobacterial examples [15, 16], reports about TI events are scarce [21, 22]. Recently, the mathematical analysis of rifampicin time-series data has been developed as a new method to directly detect TI events *in vivo* [23], pointing to a frequent occurrence of this mechanism in bacteria, including the unicellular cyanobacterium *Synechocystis* sp. PCC 6803 [23].

Antisense transcription of the *nblA* region was already detected in early transcriptomic analysis of *Nostoc*, and a transcriptional unit antisense to *nblA* was defined in its transcriptomic map [14]. Because antisense transcription in the *nblA* region is conserved in other heterocyst-forming cyanobacteria, we considered the possibility (see below) that such asRNA could regulate the expression of *nblA*. Using promoter fusions to the *gfp* gene, encoding green fluorescent protein (GFP), we show that transcription from the *as_nblA* promoter is stronger than that from the *nblA* promoter. We have prepared a strain that lacks *as_nblA* and demonstrate that the amount of *nblA* transcripts and the accumulation of the NblA protein is much higher in the absence of *as_nblA*, both in response to nitrogen limitation and exposure to high light. Strains lacking *as_nblA*, accumulating high levels of NblA, are unhealthy and prone to accumulate mutations that revert their phenotype. Rifampicin time-series analysis and mathematical modeling strongly support that TI is the main regulatory mechanism of *as_nblA*. Taken together, these observations indicate a critical role of *as_nblA* in the maintenance of appropriate amounts of NblA protein, which must be kept low when the degradation of PBS is not required.

Materials and methods

Strains and growth conditions

The strains used in this work are described in Supplementary Table S1. Cultures used in the northern blots and primer

extension assays included in Fig. 1, RACE experiment (Supplementary Fig. S3B) and rifampicin addition time-series used for Fig. 4 were bubbled with an air/CO_2 mixture [1% CO_2 (v/v)] and grown photoautotrophically at 30°C in BG11 medium [24] containing ferric citrate, instead of ammonium ferric citrate, and 10 mM $NaHCO_3$. As nitrogen sources 17.6 mM $NaNO_3$ or 6 mM NH_4Cl plus 12 mM *N*-tris (hydroxymethyl) methyl-2-aminoethanesulfonic acid-NaOH buffer (pH 7.5) were used, as indicated in each case. For all other experiments, cells were grown in flasks with shaking. Nitrogen deficiency was induced by filtering, washing, and resuspending the cells in nitrogen-free BG11 medium. Standard 4000K light intensity (referred to as low light) was 50 μmol photons·m^{-2}·s^{-1}. Exposure to high light was achieved by shifting the culture flasks to 500 μmol photons·m^{-2}·s^{-1}. Darkness was achieved by wrapping the culture flasks with aluminum foil and a black plastic bag.

The *Nostoc* strains containing $SmSp^R$ genes were grown in the presence of streptomycin (Sm) and spectinomycin (Sp), 1.5 μg/ml each (liquid medium) or 3 μg/ml each (solid medium). The medium was solidified by the addition of 10 g/l of Bacto Agar (BD). *Escherichia coli* strains were grown in LB medium, supplemented with appropriate antibiotics [25].

Construction of *Nostoc* derivative strains

The plasmids and oligonucleotides used in this work are described in Supplementary Tables S2 and S3, respectively. All PCR (polymerase chain reaction) fragments to be cloned were amplified using high fidelity iProof™ DNA polymerase. The sequences of all PCR-amplified fragments were verified entirely by sequencing.

To generate vectors for the expression of a fusion between the promoters of *nblA* or *as_nblA* and a promoterless *gfpmut2* gene in *Nostoc*, the promoter regions were amplified from genomic DNA using oligonucleotides 1008 + 1115 or 1107 + 1108, respectively. The products were digested with AccI–XhoI (*nblA* promoter) or ClaI–XhoI (*as_nblA* promoter) and cloned into ClaI–XhoI-digested pSAM270 [26], rendering pIAE92 and pIAE93, respectively. pIAE92 and pIAE93 were introduced in *Nostoc* wild type by conjugation [27], generating strains that contained the corresponding plasmid inserted in the alpha plasmid.

To generate a strain lacking the *nblA* region, two overlapping fragments were amplified by PCR using genomic DNA as the template and oligonucleotides 1109 + 1110 and 1111 + 1112, respectively. The resulting products were then used as templates for a third PCR with oligonucleotides 1109 + 1112 resulting in a DNA fragment of the *nblA* genomic region that lacks the *nblA* promoter, the complete *nblA* 5′ UTR, coding sequence and 3′ UTR, and the *as_nblA* promoter (coordinates 5407030–5408106). This PCR product was digested with BamHI and cloned into the BamHI site of pCSRO [28], rendering pIAE94. pIAE94 was introduced in *Nostoc* by conjugation [27] and double recombinants were selected rendering strain Δ*nblA*. Genomic DNA was extracted [29] from clones exhibiting sucrose resistance (double recombinants). The segregation of the introduced deletion was analyzed by PCR using oligonucleotides 563 + 564 (Supplementary Fig. S4B).

Plasmids for the expression of a 3xFLAG-tagged version of NblA (NblA-3xFLAG) in *Nostoc* were constructed using pMBA20 [15] as a backbone. A segment corresponding to the *nblA* region (coordinates 5406683–5407871) was amplified using genomic DNA and oligonucleotides 514 + 1117 and cloned into pSpark™ II rendering pIAE116, used as a template for further PCR amplification of different segments. A DNA segment including the promoter of *nblA* and the *nblA* coding sequence without sequences downstream of *nblA* (coordinates 5406949–5407697) was amplified using oligonucleotides 1115 + 1191 (the last one including the sequence encoding 3xFLAG). The resulting fragment was digested with AccI and XhoI and ligated to ClaI–XhoI-digested pMBA20, rendering pIAE119. A segment containing sequences downstream of *nblA* but not the *as_nblA* promoter (coordinates 5407701–5408028) was amplified using oligonucleotides 1188 + 1189, digested with XhoI, and ligated into XhoI-digested pIAE119 rendering pIAE130. The same segment plus the sequences corresponding to the *as_nblA* promoter (coordinates 5407701–5408157) was amplified using oligonucleotides 1188 + 1190, digested with XhoI, and ligated to XhoI digested pIAE119, rendering pIAE123 (see the scheme of constructs in Fig. 3 and Supplementary Fig. S6). pIAE123 or pIAE130 were introduced in the Δ*nblA* strain by conjugation [27], generating strains that contained the corresponding plasmid inserted in the alpha plasmid.

Plasmids for the constitutive expression of *as_nblA* in *Nostoc* were constructed based on vector pMBA37, which was previously designed for expression from the *trc* promoter. pMBA37 bears unique NsiI and XhoI sites for the cloning of DNA segments between the *trc* promoter and the T1 transcriptional terminator from the *E. coli rrnB* gene [15]. Two different fragments were amplified with oligonucleotides 1116 + 1120 or 1117 + 1119, digested with NsiI and XhoI, and cloned into NsiI–XhoI-digested pMBA37, rendering pIAE97 and pIAE99, respectively. Plasmid pMBA51, containing only the *trc* promoter and the T1 terminator [15], was used as control. Each plasmid was introduced into *Nostoc* wild-type or Δ*alr0280* RNase III-defective strains [15] by conjugation [27], generating strains that contained the corresponding plasmid inserted in the alpha plasmid.

RNA isolation and analysis

Total RNA was isolated using hot phenol as described [30] with modifications [31]. When appropriate, the samples were treated with RNase-free DNase, according to the instructions of the TURBO DNA-free™ kit (Invitrogen). Northern blot hybridization was carried out according to standard procedures after RNA separation in urea-polyacrylamide gels [32, 33], using ^{32}P-labeled probes. The ^{32}P-labeled *nblA* strand-specific probe was prepared with Taq DNA polymerase using a PCR fragment generated with oligonucleotides 253 + 254 as the template in a reaction with α-^{32}P-dCTP and a single oligonucleotide (254) as primer. The ^{32}P-labeled *as_nblA* strand-specific probe was prepared in the same way using a PCR fragment generated with oligonucleotides 1116 + 1120 as template in a reaction with α-^{32}P-dCTP and a single oligonucleotide (1120) as primer. Hybridization with *rnpB* [34] probes was used as a loading and transfer control. Primer extension analysis was performed as previously described [32] using the oligonucleotides 26 (for *nblA*) or 990 (for *as_nblA*) labeled with γ-^{32}P-ATP. Images of the radioactive membranes were obtained and analyzed using a Cyclone Storage Phosphor System and OptiQuant image analysis software (Packard).

For semiquantitative reverse transcriptase-polymerase chain reaction (RT-PCR), synthesis of first strand complementary DNA (cDNA) was performed using Superscript III™ following the manufacturer's instructions, with 1 μg of total RNA as template and using the oligonucleotides 1303 for *nblA* mRNA, 493, 1115, 1118, or 1188 for *as_nblA* RNA, and 1209 for *rnpB* in a total volume of 20 μl. After dilution to 30 μl and desalting, 1 μl of the reverse transcription (RT) product was used as a template in the PCR reactions. PCR was performed using oligonucleotide pairs 1304 + 1305 for *nblA* mRNA (27 cycles), 499 + 1188 (Fig. 3, 22 cycles) or 519 + 1118 (Supplementary Fig. S3, 30 cycles) for *as_nblA* RNA, and 1226 + 1227 for *rnpB* (22 cycles).

3′-RACE assays were performed essentially as described [35], with 2.5 μg of dephosphorylated total RNA (rAPid Alkaline phosphatase, Roche) extracted from cells incubated for 12 h in the absence of combined nitrogen, incubated for 4 h in the dark, or incubated for 30 min under high light. The 3′RNA-adapter (15 pmol) was ligated to the dephosphorylated RNA by incubation at 25°C for 2 h with T4 RNA ligase (New England Biolabs). After phenol/chloroform extraction and isopropanol precipitation, the RNA was reverse-transcribed with Superscript III™ (Invitrogen) using 2 pmol of oligonucleotide 281, which is complementary to the 3′RNA-adapter. The products of reverse transcription were amplified by PCR using MyTaq DNA Polymerase (Bioline) with oligonucleotides 282 (nested to 281) and gene-specific oligonucleotide 990, using 1 μl of the reverse transcription reaction as a template. PCR products were purified on an agarose gel and cloned into the pSpark™ TA cloning vector. Nine clones from the nitrogen stress sample and 10 clones from the high-light stress sample were sequenced.

For RNA stability analysis shown in Fig. 4, 650 ml culture of *Nostoc* cells growing in the presence of ammonium or 9 h after nitrogen removal were used. The cells in a 50-ml sample were collected in a Millipore nitrocellulose filter (0.45 μm pore diameter) and the filter was immediately frozen in liquid N_2 (sample labeled time 0). Rifampicin was added to the remaining 600 ml to a final concentration of 500 μg/ml (300 mg in 3 ml of dimethyl sulfoxide) and samples were taken as described above at 0.5, 1, 2, 4, 6, 8, 10, 15, and 30 min following the addition of rifampicin. All samples were filtered and frozen as described for time 0 and stored at −80°C until RNA extraction. A 197-bp-long barcoded spike-in RNA mix was created by *in vitro* transcription (MEGAshortscript, Thermo Fisher) of PCR-amplified fragments from the PhiX174 bacteriophage genome as described previously [36]. Twenty-three fmol of the spike-in RNA mix was added per 1 μg of total RNA. RNA samples were treated with TURBO DNA-free™ kit (Invitrogen), and strand-specific libraries were prepared using the Illumina Stranded TOTAL RNA preparation RIBO-ZERO PLUS kit and sequenced on the Illumina platform NovaSeq 6000 SP at the Genomics Core Facility of Cabimer (Seville, Spain). Raw RNA-seq data can be accessed in the GEO database under accession number GSE299220.

For RNA samples used in calculation of half-life shown in Fig. 4C, 180 ml culture of *Nostoc* cells bearing pIAE123 or pIAE130 growing in flasks in the presence of nitrate and subjected to 1 h of 700 μmol photons·m^{-2}·s^{-1} were used. The cells in a 20-ml sample were collected in a Millipore nitrocellulose filter (0.45 μm pore diameter) and the filter was immediately frozen in liquid N_2 (sample labeled time 0). Rifampicin was added to the remaining 160 ml to a final concentration of 500 μg/ml (80 mg in 0.8 ml of dimethyl sulfoxide) and samples were taken as described above at 1, 2, 4, 6, 8, 10, 15, and 30 min following the addition of rifampicin. RNA was isolated, treated with DNase, and synthesis of first strand cDNA was performed using Superscript III™ following the manufacturer's instructions, with 0.9 μg of total RNA as template and using oligonucleotides 1303 for *nblA* and 1209 for *rnpB* in the same reaction. Quantitative PCR (qPCR) was performed using SsoAdvanced™ Universal Inhibitor-Tolerant SYBR® Green Supermix (Bio-Rad #152-5017) following the manufacturer's instructions for the Bio-Rad CFX96 Cycler. The amplicons used were obtained using oligonucleotides 1501 + 1502 (*nblA*) and 1226 + 1227 (*rnpB*). For each data timepoint *nblA* Cq values were substracted by the respective *rnpB* control Cq values. Final expression values were calculated by

$$\mathrm{Exp} = 2^{[-(C_q nblA - C_q rnpB)]}$$

The resulting expression values were fitted to the simple delayed decay or the rifampicin sensitive termination (RST) model from Wanney *et al.* [23] using the R *nls* function with the inverse square root of the expression values as weights to prevent overestimation of the early values. We evaluated which model represents the data better using the Bayesian information criterion BIC, which supported the RST model for the plAE123 data (BIC; simple: −174.4772; RST: −196.1046) and the simple model for plAE130 (BIC; simple: −199.8851; RST: −194.1043).

RNA bioinformatic analysis

Raw RNA-seq data from *Nostoc punctiforme* PCC 73102 [37, 38], *Nodularia spumigena* UHCC 0039 [39], and *N. spumigena* CCY9414 [40] were downloaded from the NCBI Sequence Read Archive under the accession numbers SRR8435111, SRR8435116, SR8435121, SRR15276499, SRR5053804, SRR5053806, SRR5053809, SRR696127, and SRR1572178. Reads were mapped to the *N. punctiforme* PCC 73102 (ASM2002v1), *N. spumigena* UHCC 0039 (ASM305447v1), and *N. spumigena* CCY9414 (ASM34056v3) genomes using HISAT2 [41] as described for the treatment of *Nostoc* sp. PCC 7120 data [14].

For RNA stability analysis, reads were mapped to the *Nostoc* genome (ASM970v1) using BWA-MEM [42]. The sequencing depth at each position was calculated using samtools-depth [43] and averaged into segments of 25 nucleotides. Reads associated with the spike-in RNAs were counted using featureCounts [44] and this data was later used by DESeq2 to calculate the size factors needed for the normalization of the samples [45]. The transcription rates, half-life of the transcripts, and TI events were calculated using the Rifi R package [23]. We used the different bins covering the *nblA* gene to calculate a mean half-life and to assess whether mRNA stability differs significantly between NH_4^+ and N_2 conditions [$t½ = \ln(2)/\lambda$, where λ is the decay constant estimated by the NLS fit]. A paired Wilcoxon signed-rank test was applied directly to the per-bin half-lives ($P = .0078$, $n = 8$ bins), treating bins as approximate replicates of transcript stability. Bin-level estimates are approximately independent because the transcriptional delay parameter absorbs the position-dependent rifampicin effect, reads from non-overlapping bins

partly derive from physically distinct molecules with independent Poisson counting noise, and the paired design mitigates residual correlation shared between conditions at the same position.

Bayesian ODE model of RNA dynamics

Model overview: We developed a mechanistic ordinary differential equation (ODE) model to describe the dynamics of *nblA* mRNA (RNA, R), its asRNA (asRNA, asR), and NsrR1 (sRNA, S) under nitrogen starvation conditions. The model integrates three regulatory mechanisms: TI between convergent sense and antisense transcription, post-transcriptional regulation via sRNA-mediated RNA decay, and time-varying transcription rates. Parameters were estimated using Bayesian inference by fitting simultaneously to multiple data types while accounting for measurement-specific uncertainties.

Modeled reactions: The model captures the following biochemical processes:

Synthesis:

- RNA is transcribed at effective rate syn_R_eff, reduced by TI from asRNA
- asRNA is transcribed at effective rate syn_asR_eff, reduced by TI from RNA
- sRNA is transcribed at rate syn_S_eff

Degradation:

- Free RNA degrades at rate λ_Rfree
- Free sRNA degrades at rate λ_Sfree
- asRNA degrades at rate λ_asR
- RNA–sRNA complexes degrade at rate λ_complex

Complex formation (RNA–sRNA interaction):

RNA + sRNA ⇌ RNA·sRNA complex with association and dissociation rate constants that define the dissociation constant K_d = k_off / k_on (see QSSA below).

State variables: the model tracks three molecular species over time:

- R_tot: total RNA (free RNA + RNA·sRNA complex)
- S_tot: total sRNA (free sRNA + RNA·sRNA complex)
- asR_tot: total antisense RNA (based on experimental findings asRNA does not form a stable complex in this model)

Quasi-steady-state approximation (QSSA):

RNA–sRNA complex formation and dissociation are assumed to be fast relative to synthesis and degradation, justifying a QSSA [46]. The dissociation constant is defined as:

- K_d = k_off / k_on,

where k_on and k_off are the association and dissociation rate constants, respectively. Under the QSSA, the complex concentration C at any instant is obtained analytically by solving the binding equilibrium:

- $C = \{(R\_tot + S\_tot + K\_d) - \sqrt{[(R\_tot + S\_tot + K\_d)^2 - 4 \cdot R\_tot \cdot S\_tot]}\}/ 2$

Free species concentrations are then recovered as

- R_free = R_tot – C
- S_free = S_tot – C
- K_d is a free parameter estimated by the model.

Time-varying transcription rates:

Transcription rates change over the 24-h nitrogen starvation time course. We model this using piecewise-linear interpolation between anchor points at $t = 0$, $t = 9$ h, and $t = 24$ h:

- f_R(t): dimensionless multiplier for RNA transcription, normalized to 1.0 at $t = 0$
- f_asR(t): dimensionless multiplier for asRNA transcription, set to 102.2 at $t = 0$ [relation to f_R($t = 0$) based on reporter assays]
- f_S(t): dimensionless multiplier for sRNA transcription, normalized to 1.0 at $t = 0$.

Explicitly: $f(t) = v_0$ for $t \leq 0$; $v_0 + (v_9 - v_0) \cdot t/9$ for $0 < t \leq 9$; $v_9 + (v_{24} - v_9) \cdot (t - 9)/15$ for $9 < t \leq 24$; and v_{24} for $t > 24$, where v_0, v_9, and v_{24} are the values at the three anchor points. The raw synthesis rates entering the ODE system are therefore:

- syn_R_raw(t) = base_syn · f_R(t)
- syn_asR_raw(t) = base_syn · f_asR(t)
- syn_S_raw(t) = base_syn_S · f_S(t).

The anchor values f_RNA_0, f_RNA_9, f_asRNA_0, f_asRNA_9, and f_asRNA_24 are informed directly by GFP reporter assay data (Data Type 4 below); f_RNA_24, f_sRNA_9, and f_sRNA_24 are free parameters estimated by the model.

Transcriptional interference:

Convergent transcription of sense RNA and asRNA results in mutual TI, whereby elongating RNA polymerases (RNAPs) from one promoter cause premature termination of transcription from the opposing promoter [47, 48]. The effective synthesis rates after TI are:

- syn_R_main = max(0, syn_R_raw − θ_asR · syn_asR_raw)
- syn_R_eff = syn_R_main + synthesis_leak
- syn_asR_eff = max(0, syn_asR_raw − θ_R · syn_R_raw),

where

- θ_asR is the efficiency with which asRNA transcription causes premature termination of RNA transcription (estimated parameter).
- θ_R is the efficiency with which RNA transcription causes premature termination of asRNA transcription (estimated parameter).
- synthesis_leak represents basal RNA production that escapes TI, accounting for the presence of prematurely terminated RNA.

Because asRNA synthesis is ∼102-fold higher than RNA synthesis at $t = 0$, a θ_asR ∼0.01 results in nearly complete suppression of sense transcription. The synthesis_leak parameter permits low-level RNA accumulation under strong asRNA-mediated blocking. We assume that the asRNA likely blocks all full-length RNA synthesis at $t = 0$, but that premature terminated RNA exists in the cell, which lead to detectability at low levels in the RNAseq data. In the sRNA knockout condition, syn_S_raw is set to 0, eliminating synthesis of the sRNA and hence interaction with the RNA. In the asRNA knockout condition, syn_asR_raw is set to 0, eliminating TI.

Differential equations

Combining the above, the system evolves according to

- $dR\_tot/dt = syn\_R\_eff - \lambda\_Rfree \cdot R\_free - \lambda\_complex \cdot C$
- $dS\_tot/dt = syn\_S\_eff - \lambda\_Sfree \cdot S\_free - \lambda\_complex \cdot C$
- $dasR\_tot/dt = syn\_asR\_eff - \lambda\_asR \cdot asR\_tot$,

where C, R_free, and S_free are obtained from the QSSA at each time point as described above.

Condition-specific initial conditions

Initial conditions are computed as analytical steady-state solutions, ensuring the system begins at equilibrium for each genetic background:

- Wild type (WT): full TI active; sRNA-mediated decay active
- sRNA knockout: syn_S_raw = 0 (no sRNA); TI still active
- asRNA knockout: syn_asR_raw = 0 (no TI); sRNA-mediated decay active.

This approach avoids arbitrary initial condition choices and ensures biological consistency across conditions.

Estimated parameters

The following parameters are estimated from the data via Bayesian inference:

K_d (RNA–sRNA dissociation constant), λ_Rfree (decay rate of free RNA), λ_Sfree (decay rate of free sRNA), λ_complex (decay rate of RNA–sRNA complex), λ_asR (decay rate of asRNA), base_syn [basal RNA/asRNA transcription rate, i.e syn_R_raw($t = 0$)], base_syn_S (basal sRNA transcription rate at $t = 0$), θ_asR (TI efficiency of asRNA on RNA transcription), θ_R (TI efficiency of RNA on asRNA transcription), synthesis_leak (basal RNA escaping TI), f_RNA_9 & f_RNA_24 (RNA transcription multipliers at $t = 9$ h, $t = 24$ h), f_asRNA_9 & f_asRNA_24 (asRNA transcription multipliers at $t = 9$ h, $t = 24$ h), f_sRNA_9 & f_sRNA_24 (sRNA transcription multipliers at $t = 9$ h, $t = 24$ h), and measurement noise per data type (σ_rnaseq, σ_microarray, σ_qpcr, σ_nb1, σ_decay, σ_reporter).

Fitting data sources and connection to model variables

We fit the model to fold-changes and ratios rather than absolute expression values, because different measurement technologies (RNA-seq, microarray, northern blot, RT-PCR) have incompatible absolute scales due to differences in sensitivity, dynamic range, and normalization. Relative changes are more reproducible and biologically meaningful, and allow the model to be constrained without requiring knowledge of technology-specific scaling factors. All observations are modeled with lognormal likelihoods:

$\log(\text{observed ratio}) \sim \text{Normal}(\log(\text{predicted ratio}), \sigma)$

The following observed data contribute to the joint log-likelihood, each constraining the model by comparing experimental measurements to predicted values of state variables, their ratios, or derived quantities such as effective decay rates:

1. RNA-seq ratios at $t = 0$ and $t = 9$ h (this work and Mitschke *et al.* [9]): At $t = 0$, the observed asRNA/RNA ratio was 1152/19.9 = 57.9 and the sRNA/RNA ratio was 3098/19.9 = 155.7 (sRNA from dRNA-seq). At $t = 9$ h, the asRNA/RNA ratio was 1017/923 = 1.1. These ratios constrain the relative abundances of the three species and anchor the initial condition balance. The dramatic shift in asRNA/RNA ratio from 57.9 at $t = 0$ to 1.1 at $t = 9$ h reflects the transition from TI-dominated (low RNA) to sRNA-decay-dominated (higher RNA) regulation. Noise parameter: σ_rnaseq.
2. RNA-seq RNA fold-change, WT $t = 0$ to $t = 9$ h (this work): RNA_t0 = 19.9, RNA_t9 = 923, giving an observed fold-change of 46.4. This constrains R_tot($t = 9$)/R_tot($t = 0$) for the WT trajectory and anchors the dynamic range of RNA induction. Noise parameter: σ_rnaseq.
3. Northern blot time series for WT and sRNA knockout (Fig. 5C and Álvarez-Escribano *et al.* [10]): For the WT condition, raw signal values at $t = 0, 3, 6, 9, 12$, and 24 h were 1, 9, 14, 19, 18, and 7 (arbitrary units), normalized to $t = 3$ h, giving fold-changes of 14/9, 19/9, 18/9, and 7/9 at t = 6, 9, 12, and 24 h, respectively. For the sRNA knockout, raw values at $t = 0$, 2, 4, 6, and 8 h were 1, 5.76, 9.77, 38.1, and 46.9, normalized to $t = 2$ h, giving fold-changes of 9.77/5.76, 38.1/5.76, and 46.9/5.76 at $t = 4$, 6, and 8 h, respectively. Reference timepoints of $t = 3$ h (WT) and $t = 2$ h (sRNA KO) were chosen because the t = 0 signal was near the detection limit. These data constrain the shape of the WT and sRNA KO RNA trajectories. Noise parameter: σ_nb.
4. The GFP reporter assay values (Fig. 2B): f_asRNA_9 = 120.7, f_asRNA_24 = 96.7, and f_RNA_9 = 10.89 (all relative to $t = 0$ RNA transcription) directly inform the transcription multiplier parameters at $t = 9$ h and $t = 24$ h. Noise parameter: σ_reporter (GFP reporter values).
5. RT-PCR fold-changes for the asRNA knockout (Fig. 3C): In the asRNA KO condition, raw signal values were 1.82 at $t = 0$ and 4.47 at $t = 9$ h, giving an observed fold-change of 4.47/1.82 = 2.46. The ratio of asRNA KO to WT at $t = 9$ h was 4.47/0.805 = 5.55. These constrain the magnitude of TI (θ_asR) by quantifying how much RNA increases when asRNA-mediated interference is absent. Noise parameter: σ_qpcr (RT-PCR ratios).
6. Cross-strain ratios (northern blot and RT-PCR): WT/sRNA KO ratio at $t = 6$ h was 14/38.1 = 0.37, reflecting that sRNA KO RNA exceeds WT at this timepoint due to loss of sRNA-mediated decay. The asRNA KO/WT ratio was 4.47/0.805 = 5.55 at $t = 8$ h and 3.35/1.31 = 2.56 at $t = 24$ h, reflecting the progressive reduction of TI impact as RNA synthesis increases during nitrogen starvation. These constrain the regulatory effect sizes of sRNA-mediated decay (WT *versus* sRNA KO) and TI (asRNA KO *versus* WT). Noise parameters: σ_nb (northern blot) and σ_qpcr (RT-PCR).
7. Microarray relative changes [26]: RNA, sRNA, and asRNA signals at $t = 6$, 8, 12, 24 h were 11.24, 12.55, 14.32, 6.45 (RNA); 0.272, 0.332, 0.321, 0.779 (sRNA); and 1.181, 0.590, 0.727, 0.946 (asRNA),respectively, all expressed relative to $t = 6$ h. These constrain the temporal dynamics of all three species simultaneously across the time series. Ratios relative to $t = 0$ were not used due to low nblA expression at $t = 0$ being at or near microarray background. Noise parameter: σ_microarray.

8. Effective decay rate measurements (Fig. 4A): The apparent decay rate of RNA was measured at $t = 0$ (13.73 h^{-1}) and $t = 9$ h (4.4 h^{-1}). The model predicts the effective decay rate as:

$\lambda\_eff(t) = (\lambda\_Rfree \cdot R\_free(t) + \lambda\_complex \cdot C(t))/R\_tot(t)$

The decay rate decrease reflects the transition from sRNA-excess conditions at $t = 0$ (high complex fraction, fast apparent decay) to sRNA-depleted conditions at $t = 9$ h (more free RNA, slower apparent decay). Noise parameter: σ_decay.

9. Informed $t = 0$ ratio for asRNA KO *versus* WT: WT RNA is below the northern blot detection limit at $t = 0$, while the asRNA KO signal is detectable (1.82 au). Since the observed asRNA KO/WT ratio decreases from 5.55 at $t = 8$ h to 2.56 at $t = 24$ h, the ratio at $t = 0$ must be substantially larger than 5.55. We model this as a lognormal likelihood centered on 20 with $\sigma = 0.7$ (log scale), representing a conservative lower bound on the ratio R_tot_asRNA-KO($t = 0$)/R_tot_WT($t = 0$).

Inference and convergence

The model was implemented in Stan [49] using the cmdstanr interface [50] in R version 4.3.2 and cmdstan 2.34.1. Sampling used the No-U-Turn Sampler with 8 chains, each with 2000 warmup and 2000 sampling iterations (adapt_delta = 0.95; max_treedepth = 15; seed = 42; 16 000 total post-warmup samples). Convergence was assessed using the split $\hat{R}$ statistic and effective sample size (ESS). All parameters showed $\hat{R} \leq 1.002$ and both bulk and tail ESS exceeding 4255. A minor fraction of iterations (0.12%, 16/16 000) resulted in divergent transitions; visual inspection confirmed these were randomly distributed throughout the posterior and did not cluster near boundaries, suggesting they reflect stochastic numerical limitations in the ODE solver rather than systematic posterior geometry problems. The fitted model R object and the scripts are available at GitHub (https://github.com/JensGeorg/Bayesian-modeling-of-nblA-regulation.git) and Zenodo (https://doi.org/10.5281/zenodo.19221631).

Fluorescence microscopy

The fluorescence of filaments of *Nostoc* (wild type, Δ*nblA*, or strains bearing plasmids pIAE92, pIAE93, or pIAE123) growing for 4–5 days on solidified nitrogen-free medium supplemented with appropriate antibiotics was analyzed as described [51] using a Leica HCX PLAN-APO 63_ 1.4 NA oil immersion objective attached to a Leica TCS SP2 confocal laser-scanning microscope (Fig. 2) or an Olympus FLUOVIEW FV3000 confocal laser-scanning microscope equipped with an UPlanApo 60x/1.5 NA oil immersion objective (Supplementary Fig. S4C). Samples were excited at 488 nm, and the fluorescent emission was monitored by collection across windows of 500–538 nm (GFP) and 630–700 nm (cyanobacterial autofluorescence) (Fig. 2 and Supplementary Fig. S4C). Lambda scan analysis of *Nostoc* filaments carrying plasmids pIAE123 or pIAE130 growing for 4–5 days on top of solidified nitrogen-free medium supplemented with appropriate antibiotics was carried out using an Olympus FLUOVIEW FV3000 confocal laser-scanning microscope equipped with an UPlanApo 60x/1.5 NA oil immersion objective (Supplementary Fig. S5). Samples were excited at 488 nm and the fluorescent emission was monitored by collection in 5-nm-wide windows in the range 600–720 nm. Quantification of GFP accumulation (Fig. 2D) or single cell emission spectra (Supplementary Fig. S5B) was determined from the images using Fiji [52].

Cell fractionation and western blotting

Crude extracts were prepared using glass beads. Cells from 30 ml cultures grown to a chlorophyll content of 4–5 μg/ml were harvested by filtration, washed with 50 mM Tris–HCl buffer (pH 8), and resuspended in 500 μl of resuspension buffer (50 mM Tris–HCl, pH 8.0, 2 mM of 2-mercaptoethanol) containing a protease inhibitor cocktail (cOmplete, EDTA-free, Roche). The cellular suspension was mixed with ∼75 μl of glass beads (Sigma, 212–300 μm) and subjected to seven cycles of vortexing for 1 min followed by cooling on ice for 1 min. The cell extract was separated from cell debris and unbroken cells by centrifugation (3 min at 3000 × *g* at 4°C). The soluble fraction was obtained by centrifugation of the crude extract at 16 000 × *g* for 30 min at 4°C. The protein concentration was determined as described [53].

For western blot analysis of *Nostoc* proteins, 20–30 μg of proteins from the soluble fraction were fractionated on 10% (Fig. 2) or 15% (Fig. 3) SDS/PAGE (sodium dodecyl sulfate–polyacrylamide gel electrophoresis), transferred to nitrocellulose membranes (Transblot Turbo RTA Transfer Kit, Bio-Rad), and immunoblotted with monoclonal anti-GFP 1:5000 (Roche, #11814460001) or monoclonal anti-FLAG M2-Peroxidase (HRP) 1:5000 (Sigma #A8592) antibodies. The ECL Plus immunoblotting system (Immobilon Western Chemiluminescent HRP Substrate, Merck) was used to detect the different antibodies, using anti-mouse 1:3000 (Bio-Rad #1706516) horseradish peroxidase-conjugated secondary antibodies in the case of anti-GFP. Ponceau Red staining was used as the loading and transfer control.

Growth curve and whole cell spectra

Cells were grown under standard conditions in the presence of NO_3^- supplemented with appropriate antibiotics. Growth was monitored at different time points by the absorbance at 750 nm of samples from the different cultures mixed with an equal volume of 50% glycerol. The absorbance spectra of the different cultures were taken between 400 and 750 nm on a microplate reader (Varioskan) and normalized for the chlorophyll content by the absorbance at 680 nm after subtraction of the absorbance at 750 nm.

Isolation and analysis of suppressors of the yellow phenotype of NblA overexpressing strains

Cells containing pIAE130 inserted in the alpha plasmid were plated and grown for 15 days on solidified nitrogen-free medium supplemented with appropriate antibiotics. Genomic DNA was isolated as described [29] from individual green colonies, and the *nblA* region was amplified by PCR using oligonucleotides 59 + 68 and 5 ng of genomic DNA as template. PCR products were purified (Isolate II PCR and Gel kit, Bioline) and sequenced using the same oligonucleotides.

Results

An antisense transcript to the *nblA* mRNA is produced in heterocyst-forming cyanobacteria

The transcriptome of *Nostoc* cells growing in the presence of ammonium or subjected to nitrogen deprivation for 9 or 24 h has been previously analyzed [14] (Supplementary Fig. S1A). The transcriptional unit TU03050 corresponding to the *nblA* gene contains, in addition to the 195-nt *nblA* coding sequence, long 5′ and 3′ UTRs (Fig. 1A). Five different TSSs (TSS1 to TSS5) were previously identified for the *nblA* mRNA [9] and three of them are induced upon nitrogen deprivation [9, 10] (Fig. 1B, left panel). According to our previous data [14], a transcriptional unit (TU03051) antisense to *nblA* would also be transcribed from the region depicted in Fig. 1A. We analyzed available transcriptomic datasets for heterocyst-forming cyanobacteria [37–40] and found that long 5′ and 3′ UTRs and the presence of antisense transcription in the *nblA* region are conserved features in the heterocyst-forming cyanobacteria *N. punctiforme* PCC 73102 (Supplementary Fig. S1B), *N. spumigena* UHCC 0039 (Supplementary Fig. S1C), and *N. spumigena* CCY9414 (Supplementary Fig. S1D).

Here, we analyzed the regulation of *nblA* expression in *Nostoc* by exposure to high light intensity or darkness. Exposure to high light induced the transient expression of *nblA*, already detected after 15 min, from the three nitrogen-regulated TSSs (TSS1, TSS2, and TSS5), identified either by primer extension (Fig. 1B, middle panel) or by northern blot hybridization (Fig. 1C). The three major transcripts detected were consistent with transcription from TSS1, TSS2, and TSS5. In response to high light, expression from TSS5 was more highly induced than expression from TSS1 or TSS2. A shift to darkness produced a decrease in the low level of *nblA* expression observed under standard light conditions (Fig. 1B, right panel).

We confirmed transcription of TU03051 (renamed *as_nblA*) by primer extension (Fig. 1D) and northern blot (Fig. 1E). Primer extension with an oligonucleotide corresponding to the end of the *nblA* sequence (#990 in Fig. 1A) resulted in the detection of a main band whose size is in agreement with a transcript that starts at the TSS located previously by dRNA-seq at position 5408038r [9]. Northern blot hybridization showed a major band with a size also consistent with the length annotated for TU03051 (840 nt) [14] and several additional smaller bands that could result from processing of the main transcript or premature termination. The expression of *as_nblA* was only transiently repressed upon nitrogen removal or high-light conditions, but induced upon exposure to darkness (Fig. 1D and E). The size of the largest band detected in the northern blots indicates that *as_nblA* completely overlaps the *nblA* gene.

Sequence conservation in the promoter regions upstream *nblA* across different cyanobacterial strains is shown in Supplementary Fig. S2. No conserved sequence corresponding to binding of NtcA, known to regulate *nblA* induction upon nitrogen removal [9], is observed. However, other conserved sequences are found upstream of TSS1, 2, and 5. The position of conserved sequences is compatible with binding of transcriptional activators in the case of TSS1, 2, and 5, but in the case of TSS5 additional conserved sequences overlapping the −10 region suggest a transcriptional repressor. In fact, the conserved sequences overlapping −10 region in TSS5 are similar to the described binding site of the RpaB regulator [11], which has been identified as regulator of *nblA* in unicellular strains [2].

The 3′ end of *nblA* transcripts produced either upon nitrogen deficiency or exposure to high light was analyzed by RACE, and the results indicate that termination is most frequent around 91–94 nt after the stop codon of *nblA* (Supplementary Fig. S3, white asterisk inside the gray arrow depicting TU03050 in Fig. 1A). As expected, and in agreement with the primer extension shown in Fig. 1B, a very weak band was detected in RACE using RNA isolated from cells incubated in the dark (Supplementary Fig. S3B). The extension of *as_nblA* was analyzed by RT-PCR using oligonucleotides at three different positions to generate cDNA. The results (Supplementary Fig. S3D) indicate that the 3′ end of the *as_nblA* transcripts reaches the position of TSS1, and, to a lesser extent, even further upstream, since a faint band was observed even using cDNA generated with oligonucleotide #1115 (see scheme in Supplementary Fig. S3A). Therefore *as_nblA* entirely overlaps the *nblA* transcripts in the antisense disposition.

Expression of *nblA* and as_*nblA* in nitrogen-fixing filaments of *Nostoc*

To analyze expression of *nblA* and its antisense transcript, *as_nblA*, we prepared plasmids bearing the promoter regions of TU03050 (*nblA*) (pIAE92) or TU03051 (*as_nblA*) (pIAE93) fused to the gene encoding GFP (see scheme in Fig. 2A). The plasmids were introduced in *Nostoc* by conjugation and expression of GFP from each promoter region was analyzed by western blot using anti-GFP antibodies. GFP was barely detectable in extracts from ammonium-grown cells bearing the P_{nblA}–*gfp* fusion (pIAE92) and ammonium removal led to accumulation of GFP (Fig. 2B). In contrast, a much higher amount of GFP was detected in the case of cells containing the P_{as_nblA}–*gfp* fusion (pIAE93) both in the presence or absence of ammonium (Fig. 2B), indicating unregulated expression of *as_nblA*. GFP expression in cells bearing pIAE92 or pIAE93 was also analyzed along filaments growing on nitrogen-free plates by confocal fluorescence microscopy (Fig. 2C). Expression of GFP in filaments containing the P_{nblA}–*gfp* fusion (pIAE92) was stronger in heterocysts than in vegetative cells (Fig. 2C and D), whereas expression of GFP in filaments containing the P_{as_nblA}–*gfp* fusion (pIAE93) was comparatively very strong but unpatterned along the filaments (Fig. 2C). Figure 2D shows the quantification of the green (GFP) and red (chlorophyll autofluorescence, shown in magenta) signals in filaments of cells bearing pIAE92. Three heterocysts are indicated in the image; two of them (1 and 3) show reduced autofluorescence, an indication of maturity, whereas a heterocyst located at an intermediate position with respect to the two mature heterocysts (2) would be at an earlier stage of differentiation according to the presence of red autofluorescence.

Transcription of an antisense to *nblA* affects NblA accumulation and degradation of phycobiliproteins

We hypothesized that the transcription of *as_nblA* might affect the expression of *nblA* and contribute to the regulation of NblA accumulation in *Nostoc*. To test this hypothesis, we first prepared a strain in which the entire region encoding both TU03050 (*nblA*) and TU03051 (*as_nblA*) was deleted, so that neither *nblA* nor *as_nblA* would be

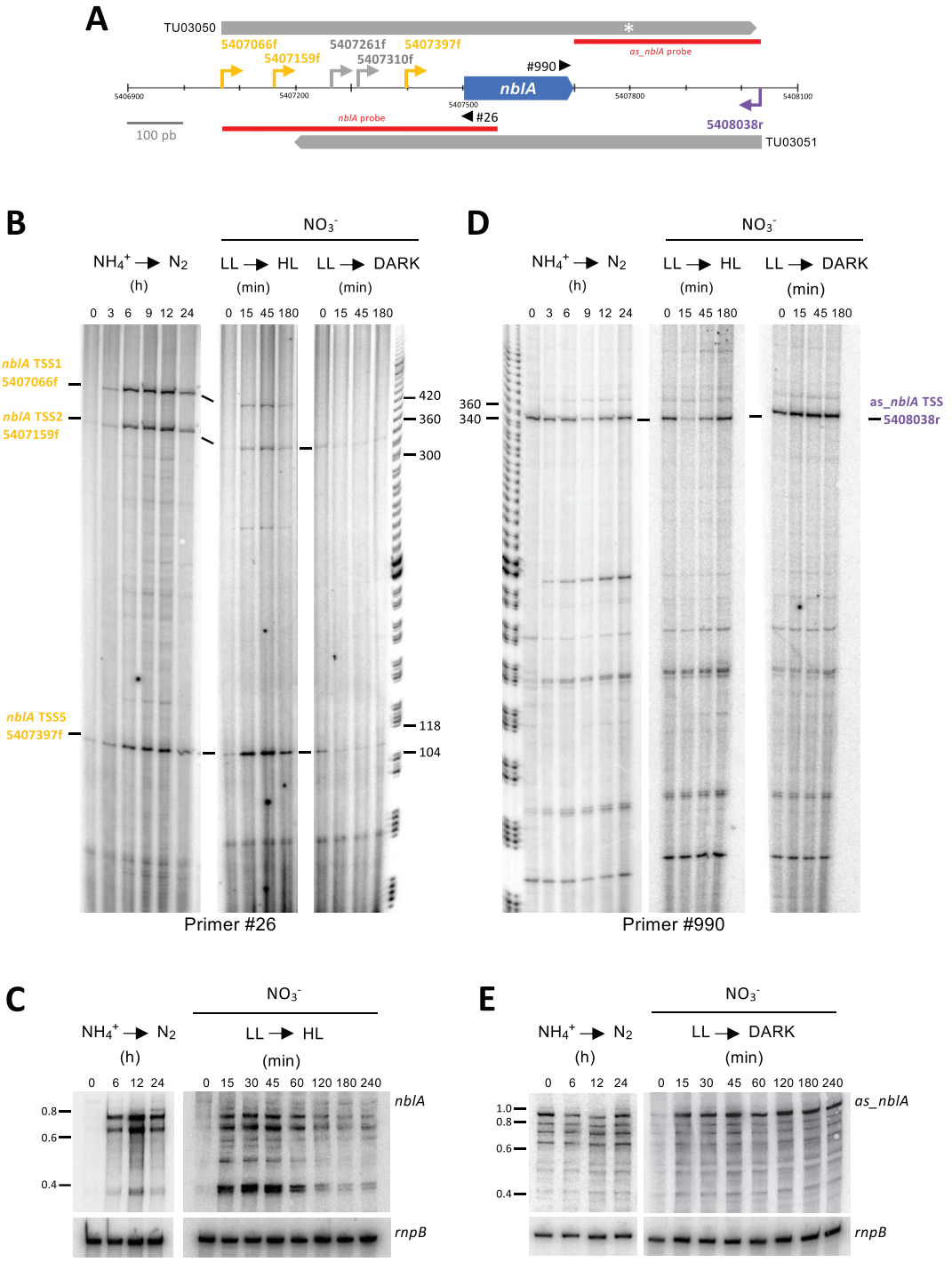

Figure 1. Transcription regulation in the *nblA* region. (**A**) Scheme of the *nblA* region from *Nostoc*. *nblA* is represented by a blue arrow. The predicted transcriptional units (TU) [14] are represented by gray arrows, with their corresponding identifications. The transcriptional start sites (TSSs) identified by dRNA-seq are indicated by bent arrows and their genomic coordinates [9] are shown. The white asterisk indicates the most frequent termination site of the *nblA* mRNA according to 3′RACE. The black triangles indicate the positions of the primers used for the primer extension assays shown in panels (B) and (D), and in Fig. 3C and D. The red bars indicate the probes used in the northern blots shown in panels (C) and (E). (**B**) Primer extension assays of *nblA* with RNA extracted from wild-type cells grown in the presence of NH_4^+ and after different times in the absence of combined nitrogen (left), grown in the presence of NO_3^- at low light (LL) and incubated under high light (HL) for the indicated times (middle), or grown at LL and incubated in the dark for the indicated times (right). The nitrogen induced TSSs in *nblA* and their coordinates are indicated in orange on the left. (**C**) Northern blot of RNA extracted from wild-type cells grown in the presence of NH_4^+ or at the indicated times after removal of NH_4^+ (left) or grown under LL and incubated under HL for the indicated times (right), fractionated in a 6% urea polyacrylamide gel and hybridized with a probe for *nblA*. *rnpB* was used as the loading and transfer control. Size markers are indicated in kb. (**D**) Primer extension assays of *as_nblA* with RNA extracted from wild-type cells grown in the presence of NH_4^+ and after different times in the absence of combined nitrogen (left), grown in the presence of NO_3^- at LL and incubated under HL for the indicated times (middle), or grown at LL and incubated in the dark for the indicated times (right). The *as_nblA* TSS and its coordinates are indicated in purple on the right. The primers used for extension are indicated at the bottom of each gel. Size markers are indicated in nucleotides. (**E**) Northern blot of RNA extracted from wild-type cells grown in the presence of NH_4^+ or at the indicated times after removal of NH_4^+ (left) or grown under LL and incubated in the dark for the indicated times (right), fractionated in a 6% urea polyacrylamide gel and hybridized with a probe for *as_nblA*. *rnpB* was used as the loading and transfer control. Size markers are indicated in kb.

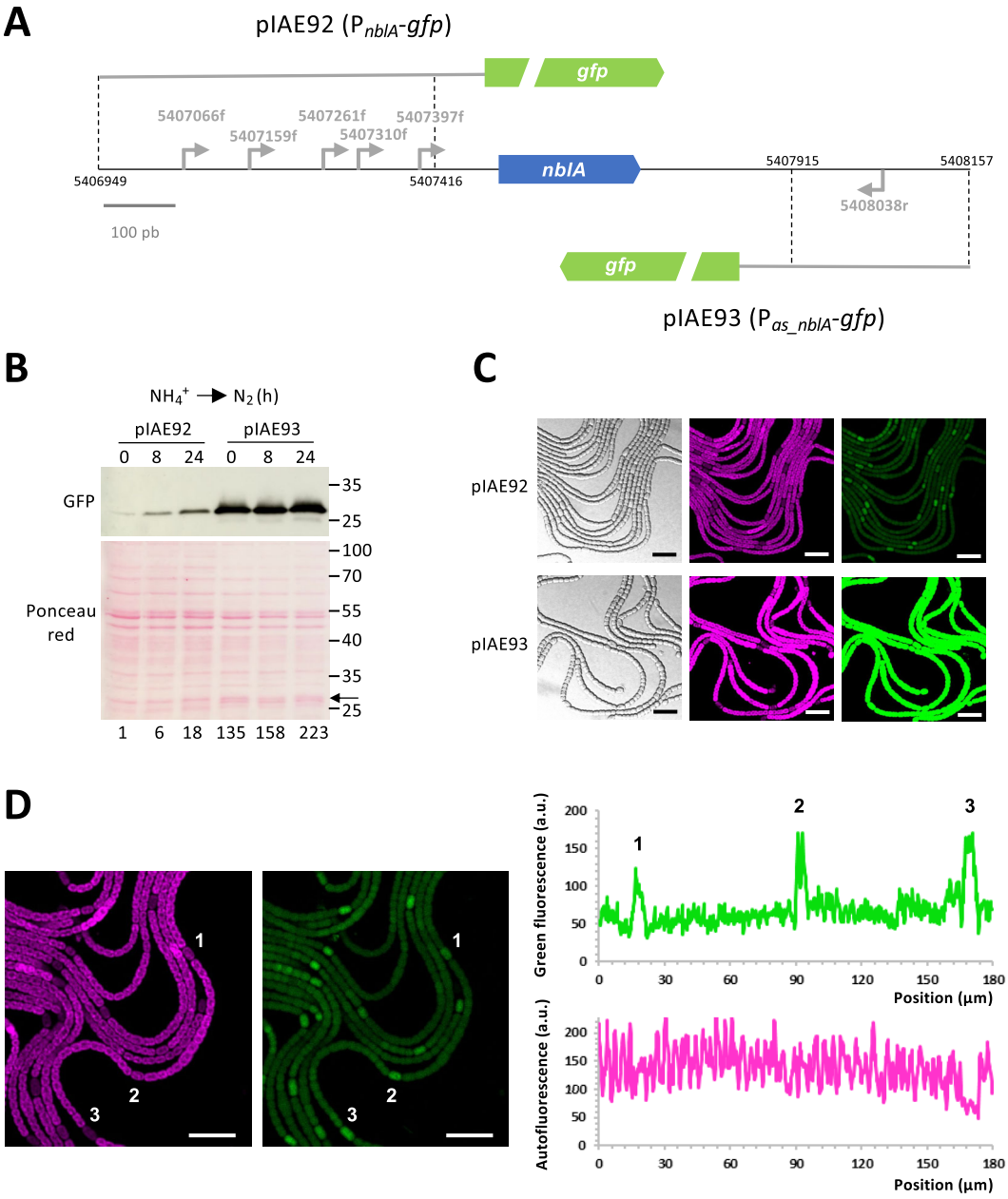

Figure 2. Expression pattern of P_{nblA} and P_{as_nblA}. (**A**) Diagram of the *nblA* genomic region. The promoter fragments used to generate transcriptional fusions with *gfp* are indicated between dashed lines. The genomic coordinates of the promoter fragments boundaries are indicated by black numbers. The coordinates and polarity of the TSSs are indicated by gray numbers. (**B**) Protein extracts from *Nostoc* cells containing pIAE92 or pIAE93 grown in NH_4^+ and then incubated for the indicated times in the absence of combined nitrogen were used for western blot with anti-GFP antibodies (top). Before blotting, the membrane was stained with Ponceau red (bottom). The black arrow indicates the position of GFP. Molecular size markers are indicated on the right in kDa. Numbers below the gel indicate the relative amount of GFP signal in each lane normalized with the Ponceau red staining and relative to the amount in strain bearing pIAE92 at $t = 0$, that was set to 1. Two different clones of each strain were analyzed in independent experiments with similar results. (**C**) Confocal fluorescence images of bright field (left), red channel, shown in magenta (middle), and green channel (right) of *Nostoc* filaments carrying the *gfp* gene under the control of the *nblA* promoter (plasmid pIAE92, top) or the *as_nblA* promoter (pIAE93, bottom) and growing on top of medium lacking any source of combined nitrogen. All images were acquired with the same sensitivity settings so that the intensities can be compared. Scale bars, 20 μm. (**D**) Quantification of the signals for the green and red (shown in magenta) channels of *Nostoc* filaments carrying the *gfp* gene under the control of the *nblA* promoter (plasmid pIAE92) is shown for the filament indicated in the images shown on the left. The heterocysts present in the quantified filament are numbered. Scale bars, 20 μm. a.u., arbitrary units. Fluorescence images are representative of at least 10 images from at least two independent experiments.

transcribed in this strain (see the scheme and verification of deletion in Supplementary Fig. S4A and B). It has been previously described that the lack of NblA leads to a phenotype characterized by heterocysts that maintain red autofluorescence, similar to vegetative cells, in contrast to the wild-type strain in which heterocysts lack red autofluorescence as a consequence of PBS degradation [8]. The mutant phenotype of the Δ*nblA* strain we constructed was therefore verified by fluorescence confocal microscopy (Supplementary Fig. S4C, middle panels). Complementation of the mutant phenotype of the Δ*nblA* strain was achieved by introducing a construct encoding a 3xFLAG-tagged version of NblA (see pIAE123 in Fig. 3A) in this strain. The lack of red autofluorescence in the heterocysts of the strain bearing pIAE123 (Supplementary Fig. S4C, right panels) indicates that the 3xFLAG-tagged version of NblA is functional and restores the reduction of the red autofluorescence phenotype observed in the heterocysts of the wild-type strain.

Two versions of the *nblA* region encoding 3xFLAG-tagged NblA were compared (see scheme in Fig. 3A). pIAE123 included both the entire *nblA* promoter and the *as_nblA* promoter, so that both the *nblA* mRNA (with its 5′ and 3′ UTRs) and *as_nblA* would be transcribed. In contrast, pIAE130 contained the *nblA* gene and its upstream and downstream regions but not the *as_nblA* promoter region. It should be noted that the most common 3′ UTR of *nblA* mRNA extends only ∼100 nt downstream the end of the coding sequence according to 3′ RACE (Supplementary Fig. S3C), therefore, deletion of the *as_nblA* promoter in pIAE130 does not alter the 3′ UTR of the *nblA* mRNA produced. In both cases, the T1 terminator of the *rrnB* gene of *E. coli* was included after the *nblA* region. Transcription of *as_nblA* was determined by RT-PCR and, as expected, took place in the strain bearing pIAE123 but not in the strain bearing pIAE130 (Fig. 3B). This result confirms that the deletion of the promoter corresponding to the TSS at position 5408038r leads to the absence of *as_nblA* transcription.

We then analyzed *nblA* expression and the accumulation of the 3xFLAG-tagged NblA protein in strains containing pIAE123 or pIAE130 in response to either combined nitrogen removal (Fig. 3C, E) or exposure to high light intensity (Fig. 3D and F). When the entire region encoding both *nblA* and *as_nblA* was present (strain bearing pIAE123), the *nblA* transcript and the NblA protein were barely detectable in the presence of combined nitrogen (lanes labeled 0) and could only be observed upon removal of combined nitrogen (lanes labeled 8 and 24) (Fig. 3C and E). This is consistent with the previously observed induction of the *nblA* promoter upon removal of combined nitrogen (Figs 1B and C, and 2B). In contrast, in the strains bearing pIAE130 (therefore lacking *as_nblA*), both the *nblA* transcript and the 3xFLAG-tagged NblA protein were observed even in the presence of combined nitrogen (lanes labeled 0). Similar observations were made in the case of *nblA* expression and NblA accumulation in response to exposure to high light (Fig. 3D and F). In this case, in the strain bearing pIAE130, both the *nblA* transcript and the 3xFLAG-tagged NblA protein were observed even in the presence of regular low light before exposure to high light intensity (lanes labeled 0). Primer extension analysis (Fig. 3C and D, top panels) indicates that transcription from TSS5, which is induced either by nitrogen removal or exposure to high light in cells bearing pIAE123, takes place in the strain bearing pIAE130 even in the presence of combined nitrogen under standard illumination (lanes labeled 0). Therefore, *as_nblA* seems to be required to suppress the background transcription of *nblA* under non-inducing conditions.

The integrity of phycobilisomes is altered in strains lacking *as_nblA*

A decrease in the amount of PBP in cell extracts of strains bearing pIAE130 could be observed in the membranes stained with Ponceau red (Fig. 3E and F, lower panels). Since PBS degradation is an indication of NblA function, this observation is consistent with the increased accumulation of NblA in the strain containing pIAE130 (Fig. 3E and F, upper panels). Liquid cultures of the strains bearing pIAE123 and pIAE130 showed a difference in color, which was yellowish in the case of cells bearing pIAE130 (that do not transcribe *as_nblA*) but green in the case of cells bearing pIAE123 (that includes the entire region encoding *nblA* and *as_nblA*) (Fig. 3G). Whole cell absorption spectra taken of cells growing in the presence of nitrate showed that the PBS content was lower in the strain bearing pIAE130 than in the strain bearing pIAE123 (Fig. 3G). We also analyzed filaments of strains bearing pIAE123 or pIAE130 by performing single-cell *in vivo* fluorescence spectra at room temperature. Cells were excited at 488 nm (a wavelength that excites phycocyanin and chlorophyll), and images were taken at 5-nm wide windows for wavelengths ranging from 600 to 720 nm. Images corresponding to 645 nm (emission of phycocyanin) and 680 nm (emission of photosystem II chlorophyll) are shown (Supplementary Fig. S5A), together with the fluorescence emission recorded for three heterocysts of each strain in the range 600–720 nm (Supplementary Fig. S5B). Comparison of the graphs shows that the peak corresponding to the fluorescence at 645 nm is missing in heterocysts of the strain containing pIAE130, an indication of a more extensive degradation of PBP in those heterocysts.

Accumulation of NblA in strains lacking *as_nblA* is deleterious

The growth rate of the strain bearing pIAE130 was reduced in comparison to that of the strain bearing pIAE123, indicating that the reduction in the PBS content under standard autotrophic growth conditions is detrimental for growth (Supplementary Fig. S6A and B). In plates containing the strain bearing pIAE130, green colonies appeared with time over the yellowish background (Supplementary Fig. S6C). Green colonies were isolated from plates lacking combined nitrogen of cells containing pIAE130, and the region encoding NblA was PCR amplified and sequenced. In all cases the amplified fragments were longer than expected. Sequencing of PCR fragments obtained from 14 different colonies revealed that they carried insertions of a transposase, identical to those present in the chromosome of *Nostoc* or in plasmids alpha, beta, or delta, in the promoter or coding sequence of *nblA* (Supplementary Fig. S6D), indicating that those transposases had been mobilized and disrupted the expression of *nblA*.

as_nblA regulates *nblA* expression through transcriptional interference

To decipher the regulatory mechanism(s) of *as_nblA*, we first explored the possibility of a co-degradation mechanism. For this purpose we generated strains expressing in *trans* two segments of *as_nblA* under the control of a strong and constitutive promoter (Supplementary Fig. S7A), an experimental

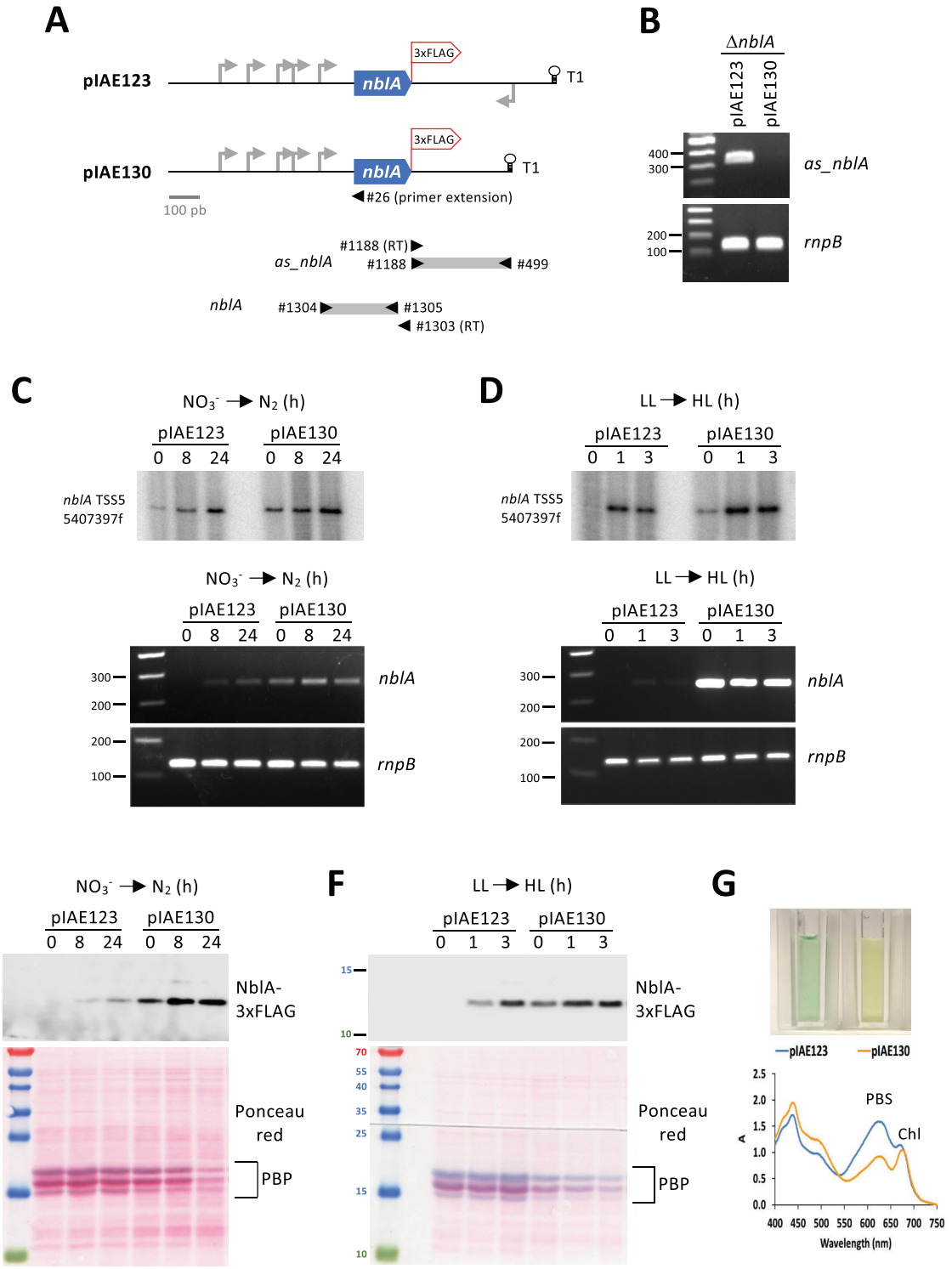

Figure 3. Effect of *as_nblA* on *nblA* expression. (**A**) Diagram of the two DNA fragments encoding 3xFLAG-tagged NblA that were introduced into the Δ*nblA* strain. The gray bent arrows indicate the five TSSs identified for *nblA* and the TSS identified for *as_nblA*. The position of the T1 transcriptional terminator is indicated by a hairpin. A scheme of the position of the oligonucleotides (black triangles) used for primer extension, reverse transcription (RT) and cDNA amplification in the RT-PCRs shown in panels (B)–(D), as well as the amplified DNA segments (gray bars) is also shown. (**B**) RT-PCR of *as_nblA* (top) and *rnpB* (bottom) with RNA extracted from the indicated strains grown in the presence of NH_4^+ under standard LL intensity. (**C**) Primer extension of *nblA* (top) and RT-PCR of *nblA* and *rnpB* (bottom) with RNA from the indicated strains grown in the presence of NO_3^- or after 8 or 24 h in the absence of combined nitrogen. (**D**) Primer extension of *nblA* (top) and RT-PCR of *nblA* and *rnpB* (bottom) with RNA extracted from the indicated strains grown in standard LL or after 1 or 3 h under HL. (**E**) Protein extracts from the same cells used in panel (C) were used for western blot with anti-FLAG antibodies (top). Before blotting, the membrane was stained with Ponceau red (bottom). The position of the PBP is highlighted with a bracket. (**F**) Protein extracts from the same cells used in panel (D) were used for western blot with anti-FLAG antibodies (top). Before blotting, the membrane was stained with Ponceau red (bottom). The position of the PBP is indicated with a bracket. Size markers are indicated in nucleotides (B–D) or kDa (E, F) on the left. (**G**) Image of cell suspensions of the indicated strains (top) and whole cell absorption spectra of the same suspensions (bottom). The position of the PBS or chlorophyll (Chl) absorption maxima are indicated. Two independent clones of each strain were analyzed with similar results in all cases.

approach that we have used previously to analyze antisense regulation by RNase III-dependent duplex degradation [15, 16]. The different *as_nblA* versions were introduced both in a wild-type and a *Δalr0280* strain, an RNase III deletion mutant [15]. The overexpression in *trans* of either version of *as_nblA* produced no clear reduction in *nblA* mRNA accumulation in any of the two genetic backgrounds (Supplementary Fig. S7B). This is in contrast with the clear effect observed for *as_nblA* when expressed in *cis* (Fig. 3).

The observation that *as_nblA* affects *nblA* mRNA accumulation when expressed in *cis* but not when it is transcribed in *trans* from a strong promoter suggests that a TI mechanism is involved in the regulation by *as_nblA*. The analysis of naturally occurring TI events entails genetic and technical challenges. Recently, the mathematical analysis of RNA-seq data from rifampicin time-series has been developed as a new method to detect *in vivo* TI events in bacteria [23]. Since rifampicin prevents transcription initiation but does not affect elongation, transcript levels at positions downstream of a TSS remain constant until the last elongating RNAP passes that position [54]. This leads to a delayed onset of exponential decay (the "delay") that depends on the distance to the TSS and the elongation speed. In addition to this behavior, Wanney *et al*. detected in phylogenetically diverse organisms that the abundance of some transcript fragments actually increased after rifampicin addition, which can be the consequence of rifampicin relieving termination caused by TI due to collision of RNAPs transcribing in opposite directions, generating an increase in the transcripts abundance after rifampicin addition [23].

To take advantage of this new methodology, we analyzed transcriptomic data from wild-type cells subjected to treatment with rifampicin, both in the presence of ammonium, where only basal transcription of *nblA* would be observed, or 9 h after ammonium removal, when induction of *nblA* has already taken place. Bioinformatic analysis using the "Rifi" R package [23] revealed several findings in the genomic region around *nblA* (Fig. 4).

First, in the presence of ammonium, the synthesis rate of *as_nblA* was much higher than that of *nblA*, and we detected an increase in *nblA* transcription from TSS1 9 h after nitrogen removal. These observations are consistent with results shown in Figs 1B and C, and 2. Second, the observed difference in mRNA stability was highly significant (paired Wilcoxon signed-rank test, $P = .0078$), with the mean half-life of nblA mRNA increasing approximately three-fold, rising from 3.03 min under NH_4^+ conditions to 9.46 min after combined nitrogen removal (Fig. 4A). Third, in the presence of ammonium, we detected a particularly long delay (~4 min) for the start of the exponential decay of the *nblA* transcript after the addition of rifampicin (Fig. 4B, gray shaded area in the bottom panels). This long delay suggests a significant distance of the positions analyzed from their TSS, indicating that the detected small amount of *nblA* transcripts in the presence of ammonium primarily originates from readthrough transcription of the upstream operon. Fourth, we observed a characteristic pattern of increased transcript abundance after rifampicin addition, consistent with TI, around position 5406950 in cells grown in the presence of ammonium (Fig. 4B, bottom panels, middle). This position corresponds to the end of the transcript resulting from readthrough transcription from the upstream gene *alr4516*. This characteristic pattern is detectable because this position is sufficiently far from the upstream

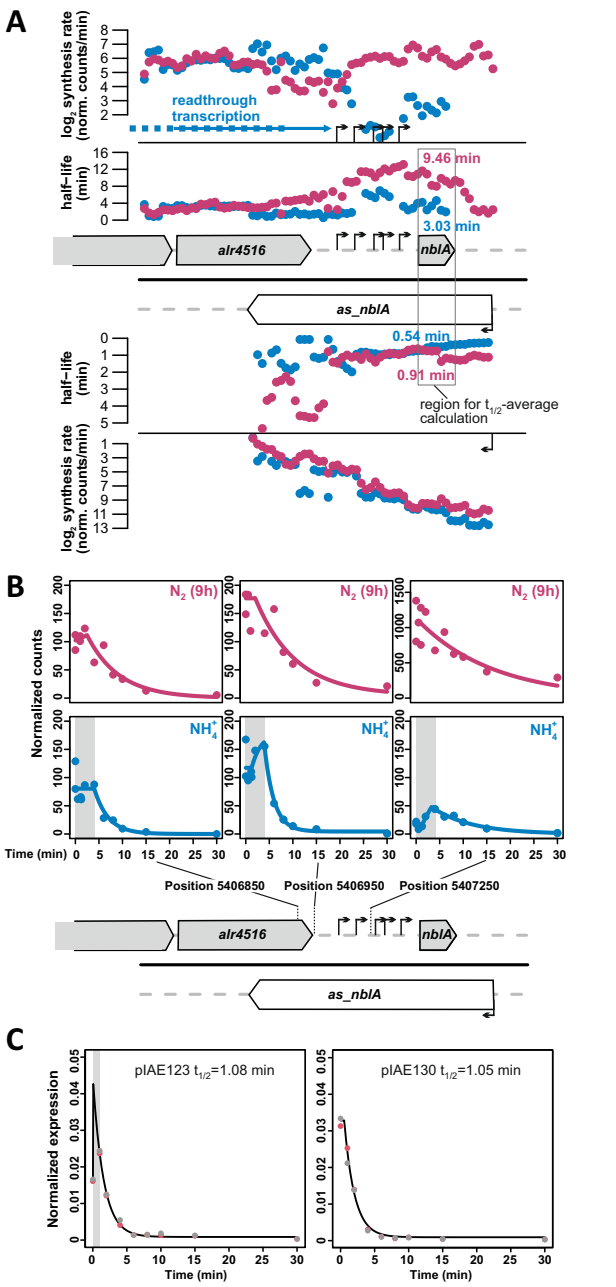

Figure 4. Analysis of *nblA* genomic region using rifampicin time-series. (**A**) Half-life and $\log_2$ calculated synthesis rate of all the 25-nt segments in the *nblA* genomic region using Rifi. Data are shown for RNA samples isolated from cultures grown in media containing NH_4^+ (blue) or 9 h after nitrogen depletion (dark pink). The coding regions of *alr4516* and *nblA* are depicted by gray arrows. The *as_nblA* transcript is shown by a white arrow. The transcription start sites of *nblA* and *as_nblA* are displayed by bent arrows [9]. For each 25-nt segment, the synthesis rate was calculated from the RNA abundances at $t = 0$ and the fitted decay constants. The half-life of *nblA* mRNA and *as_nblA* in the different conditions is shown as the half-life average of the segments contained inside of the thin gray frame that covers *nblA* and *as_nblA*. (**B**) Fitted decay curves calculated by Rifi for the 25-nt segments starting at three selected positions 5406850 (upstream the *nblA* promoters), 5406950 (promoter for TSS1), and 5407250 (downstream the TSS1 promoter). The delayed onset of exponential decay (delay) is marked in gray for the samples grown in media containing NH_4^+ (bottom panels). (**C**) Fitted decay curves of *nblA* mRNA (position 5407566–5407673) analyzed by RT-qPCR in strains bearing pIAE123 or pIAE130 subjected to 1 h of high light stress and treated with rifampicin for the indicated times. The delay is marked in gray. Two technical replicates are shown in red and gray.

transcript's TSS to be observed within the timeframe of our rifampicin time-series. Conversely, we detected no increased transcript abundance after rifampicin addition resulting from TI within the 5′UTR of *nblA* mRNA during nitrogen depletion nor delay in the start of exponential decay (Fig. 4B, position 5407250 upper panel). Under these conditions, *nblA* is strongly transcribed from its own promoters. The increased sense to antisense synthesis ratio leads to a much lower total fraction of termination by interference at this condition, which is not visible in the data anymore. In order to further test the possibility of a TI mechanism for *as_nblA*, we analyzed *nblA* accumulation after rifampicin addition in strains bearing pIAE123 and pIAE130 subjected to 1 h of high-light stress (Fig. 4C). In this case, we used RT-qPCR and an amplicon internal to *nblA* but as far as possible from the *nblA* TSSs (positions 5407566–5407673) to try to detect the characteristic increase after rifampicin addition within our timeframe resolution. No differences in *nblA* mRNA half-life between the two strains were detected, whereas a characteristic increase after rifampicin addition was only observable in the strain bearing pIAE123 (that produces *as_nblA*) but not in the strain bearing pIAE130 (that does not produce *as_nblA*).

A mathematical model of *nblA* regulation

To better understand the physiological implications of the TI mechanism exerted by *as_nblA*, we modeled the expression of *nblA* based on the data presented here and previously available experimental data. Our model for *nblA* regulation considers two key observations. First, *as_nblA* exerts its regulatory function mainly through TI as lacking the asRNA did not change the mRNA stability (Fig. 4C). Second, a significant, approximately three-fold difference was observed in *nblA* RNA stability between standard and nitrogen depletion conditions (Fig. 4A). We propose that the difference in *nblA* mRNA half-life is primarily due to the interaction and co-degradation of *nblA* mRNA with the small RNA (sRNA) NsrR1, as supported by literature [10]. A decreased translation rate for the *nblA*:NsrR1 complex was not incorporated in the model as our focus was on RNA levels.

This leads to a model (Fig. 5A) where *nblA* mRNA levels are regulated by (i) its synthesis rate, mainly driven by the three nitrogen-regulated inducible TSSs. The relative synthesis rate of *as_nblA* and *nblA* was estimated from the transcriptional fusions shown in Fig. 2. (ii) Interaction with the sRNA NsrR1 that increases the *nblA* decay. There are no quantitative data for the actual dynamics of the NtcA-dependent promoter activity of NsrR1, thus these data are fitted by the model priored by microarray expression data [26]. (iii) TI by transcription of the *as_nblA* asRNA, which directly reduces the synthesis of full-length mature *nblA* mRNA. Informed priors for RNA stability were taken from our rifampicin time-series data (Fig. 4).

Using Bayesian fitting, we demonstrate that the proposed model successfully captures the observed biological effects and describes a comprehensive set of available experimental time-series data during nitrogen depletion. These include microarray and RNA-seq expression data for *nblA*, *as_nblA*, and *nsrR1* in a WT background [14, 26], northern blot data for *nblA* in WT and NsrR1 knockout strains [10], RT-PCR data for *nblA* in strains bearing pIAE123 (wild type) or pIAE130 (lacking *as_nblA*) (Fig. 3), and observed decay constants of *nblA* at standard and nitrogen depletion conditions (Fig. 4).

Using the fitted parameters (Supplementary Table S4), we modeled the observed (free + complexed *nblA*:NsrR1) concentrations for *nblA* mRNA in the wild type, *as_nblA* knockout (Δ*as_nblA*), and NsrR1 knockout (ΔNsrR1) scenarios (Fig. 5C and Supplementary Fig. S8). In the wild type, *nblA*, *as_nblA*, and NsrR1 are all present, and TI by the asRNA effectively suppresses *nblA* expression from readthrough transcription of the upstream operon during the early phase of nitrogen depletion. A low mRNA collision termination probability of ca. 1% is sufficient to achieve this effect given the high asRNA synthesis rate (Fig. 5C). Finally, although disentangling gene expression in vegetative *versus* heterocyst cells from bulk transcriptomics is challenging, our single-cell transcriptional GFP fusion measurements (Fig. 2) allow us to estimate that the *nblA* synthesis rate is approximately three-fold higher in heterocysts compared to vegetative cells under nitrogen depletion (Fig. 2D). Incorporating this difference into our simulations reveals that the system permits rapid *nblA* induction in heterocysts (rising after ∼0.1 h), whereas vegetative cells remain at baseline levels (∼15 a.u.) for ∼0.5 h. While defining a strict critical threshold for *nblA* concentration is difficult, the steady-state levels of mutant strains with known growth phenotypes serve as anchors. The baseline *nblA* level of the ΔNsrR1 strain (∼104 a.u.), which exhibits a minor phenotype under standard conditions [10], is reached after only 0.6 h in heterocysts, compared to 2.3 h in vegetative cells. Furthermore, the baseline level of the Δ*as_nblA* strain (∼534 a.u.), which displays a severe growth phenotype, is reached after 2.2 h in heterocysts but requires 7.5 h in vegetative cells. Notably, the maximal induction in vegetative cells (∼861 a.u.) only marginally exceeds the baseline level in strain Δ*as_nblA* (Supplementary Fig. S9). Ultimately, the model predicts that the regulatory system amplifies a 3-fold difference in synthesis rate (heterocysts *versus* vegetative cells) into an ∼11.6-fold difference in maximal *nblA* concentration (Fig. 5C and Supplementary Fig. S9). The actual concentration difference is likely even greater, as NsrR1 expression is presumably lower in heterocysts due to NtcA repression, an effect not included in this model due to a lack of quantitative data.

Discussion

The proteolysis adapter NblA plays a central role in PBS degradation and must therefore be tightly controlled to balance stress adaptation with cellular homeostasis. At the transcriptional level, *nblA* induction in response to nitrogen deprivation is regulated by NtcA in *Nostoc* [9], although no consensus NtcA-binding sequence is identified in the conserved sequences upstream of the regulated TSS (Supplementary Fig. S2). This observation suggests that NtcA indirectly regulates *nblA* expression through a yet unknown transcription factor. We have shown here induction of expression of *nblA* in response to high light (Fig. 1B and C), and conserved sequences corresponding to an RpaB-binding site are located upstream of TSS5 in a position compatible with repression by RpaB (Supplementary Fig. S2), similar to the case of unicellular strains [2, 11]. At the post-transcriptional level, NblA accumulation is negatively affected by binding of an sRNA, NsrR1, preventing translation of NblA and promoting *nblA* mRNA degradation in the presence of combined nitrogen [10].

Accumulating evidence points to the physiological consequences of antisense transcription, which is widespread in cyanobacteria. In fact, the transcriptional landscape of *Nostoc*

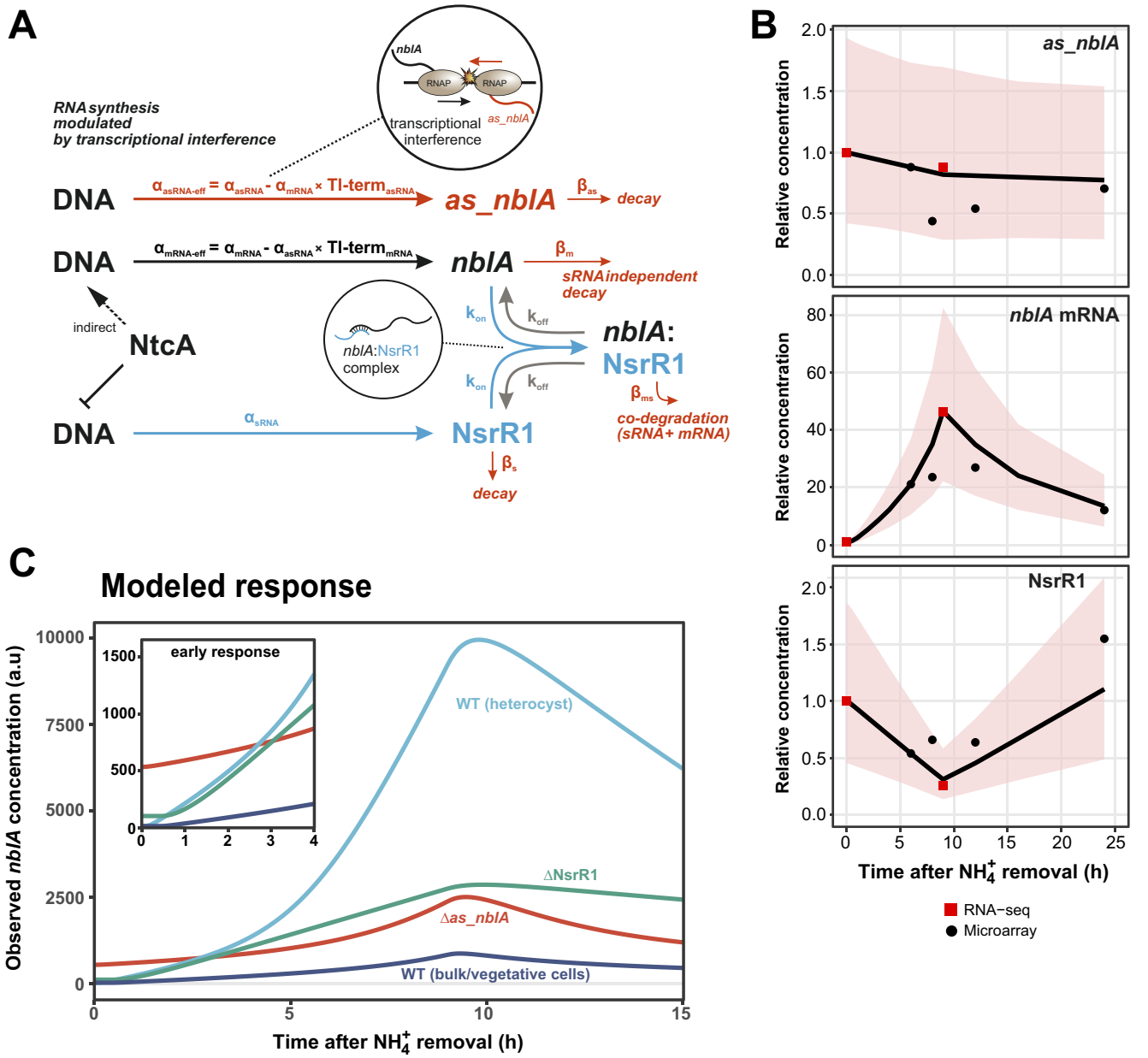

Figure 5. Mathematical modeling of *nblA* expression upon nitrogen removal. (**A**) Model for *nblA* regulation through *as_nblA* and NsrR1 corresponding to the ODEs used for the fitting described in the "Materials and methods" section. (**B**) Fitted expression posterior levels of *as_nblA*, *nblA* mRNA, and NsrR1 relative to their respective values at time 0 (means shown as black lines). The 90% confidence intervals of the fits are drawn in salmon and the original microarray data [26] and RNAseq data used for the fit are shown as black dots and red squares, respectively. Microarray data were scaled to match the model trajectory at $t = 6$ h to visualize relative dynamics, excluding unreliable $t = 0$ measurements. (**C**) Simulation of *nblA* expression in different scenarios as indicated in the plot. The parameters are taken from the fitted model. In the knockout scenarios, the synthesis rates for *as_nblA* or NsrR1 were set to 0. In the heterocyst scenario, the synthesis rate of *nblA* was, based on the experimental data (Fig. 2D), three times higher than in the vegetative cells of the wild-type strain. a.u., arbitrary units.

contains ~65% of transcripts with a segment in antisense orientation to other transcripts [14]. In this work, we show that *as_nblA* entirely overlaps the *nblA* mRNA in antisense disposition. Transcription from the promoter of *as_nblA* is much stronger than transcription from the promoter of *nblA* (Fig. 2) and takes place also in the presence of combined nitrogen and under standard illumination, a condition in which transcription of *nblA* is barely detectable. According to fluorescence microscopy of strains bearing a fusion to *gfp*, the expression of *nblA* is stronger in heterocysts than in vegetative cells (Fig. 2C and D).This observation is in agreement with the immunolocalization of NblA carried out in *Tolypothrix* sp. showing that, upon nitrogen step-down, NblA is preferentially located in the differentiated heterocysts [55], and its presence correlates with the observed reduction of autofluorescence that is characteristic of mature heterocysts but does not take place in *nblA* mutants of *Nostoc* [8] (Supplementary Fig. S4).

Detection of the native NblA protein had remained elusive in *Nostoc*, because antibodies raised against NblA from *Nostoc* were unable to detect native NblA in protein extracts of this strain [4, 10]. Therefore, we have used a functional 3xFLAG-tagged version of NblA for detection in pro-

tein extracts. A strain that contains sequences encoding both the *nblA* mRNA and the *as_nblA* (Fig. 3) showed regulated expression of *nblA* and accumulated NblA in response to either nitrogen removal or exposure to high light. In contrast, a strain in which *as_nblA* is not transcribed (Fig. 3A and B) accumulated NblA even in the presence of combined nitrogen and under regular standard light intensity (Fig. 3). These observations demonstrate the role of *as_nblA* in maintaining regulated low levels of NblA under non-stress conditions.

Unregulated high accumulation of NblA in the strain lacking *as_nblA* resulted in cultures with a yellowish color, reduced amounts of PBS, and slightly decreased growth rate even in the presence of nitrate. When plated in the absence of combined nitrogen, the colonies were yellow and showed extremely poor growth. After a few days of incubation, green colonies arose in the plates that seemed to have overcome the deleterious consequences of NblA accumulation (Supplementary Fig. S6A–C). Although the reasons for such deleterious effects are currently unknown, one possibility is that non-physiological amounts of NblA may operate the proteolytic processing of additional proteins besides PBP, since NblA is reported to interact with other proteins not related to PBP degradation [4]. In fact, a recent report describes that the ectopical overexpression of NblA encoded in cyanophages leads to proteolytic processing of additional photosynthesis-related proteins beyond PBP, as well as proteins not involved in the photosynthetic process [7]. Additionally, excess NblA might titrate the Clp protease and inhibit proper processing of other proteins. Green colonies appeared with high frequency in the strain that lacks *as_nblA*, suggesting a selective pressure to revert the deleterious effects of increased accumulation of NblA in this strain. In fact, sequencing of the *nblA* region from those green colonies revealed the insertion of different transposases, preventing the production of a functional NblA protein (Supplementary Fig. S6D). Perhaps the stress induced by the overexpression of *nblA* could activate the mobilization of some of the many transposable elements present in the genome of *Nostoc* [56]. Taken together, these observations underscore the strong selective pressure to limit NblA levels and highlight the physiological relevance of antisense-mediated control.

Antisense regulation mediated by RNA duplex degradation by RNase III has been previously described in *Nostoc* [15, 16]. When *as_glnA* or *as_gltA* were overexpressed in *trans*, almost complete degradation of their sense mRNA partners took place in the wild-type background but not in the RNase III mutant background [15, 16]. However, using the same experimental approach here, we show that the overexpression of *as_nblA* in *trans* did not reduce the amount of *nblA* mRNA (Supplementary Fig. S7). Furthermore, the absence of *as_nblA* did not significantly affect the half-life of *nblA* mRNA (Fig. 4C), suggesting that duplex degradation is not the major regulatory mechanism operated by *as_nblA*. Therefore, we explored alternative mechanisms. A recent study highlighted the role of TI in several bacteria, including the unicellular cyanobacterium *Synechocystis* sp. PCC 6803, and the authors developed an informatic pipeline for the quantitative modeling using RNA-seq of rifampicin time-series [23]. We have therefore generated a dataset from cells treated with rifampicin and applied this same procedure to its analysis. Our data support TI as the main mode of action of *as_nblA*, by limiting readthrough transcription from upstream regions (Fig. 4).

TI occurs when transcription from opposing or tandem promoters disrupts gene expression through mechanisms such as promoter occlusion, displacement of paused RNAPs or transcription factors, or physical collisions between elongating complexes [47, 48]. The exact molecular mechanisms, e.g. transcription–translation coupling and impact on DNA supercoiling, are still under investigation [57]. The regulatory potential of TI was first implicated by high-throughput transcriptomic studies revealing pervasive antisense transcription in both prokaryotes [17, 58, 59] and eukaryotes [60]. TI modulates, for instance, rifampicin sensitivity in *Bacillus subtilis* [61]. A main obstacle to large-scale TI investigation has been the absence of methods capable of distinguishing TI from other phenomena. The method used here [23] exploits a diagnostic kinetic signature unique to TI. Under steady-state conditions, antisense RNAPs continuously terminate a fraction of sense RNAPs within the sense/antisense overlap zone, depressing sense RNA levels downstream of the antisense TSS. Upon rifampicin addition, new antisense initiation is blocked, relieving antisense transcription-based termination and allowing the remaining sense RNAPs to read through the former interference zone. This results in a paradoxical post-rifampicin-treatment increase in sense RNA at positions downstream of the antisense TSS. Crucially, this method detects this signal in bulk transcriptomic data from living cells without genetic manipulation of the locus, making it applicable at genome-wide scale. Additionally, our data reveal a strongly asymmetric termination probability between sense and antisense RNAPs, which was proposed also in another study [62], consistent with a role for transcription–translation coupling in determining collision outcomes.

We have modeled the accumulation of *nblA* in response to nitrogen limitation (Fig. 5) and the model suggests that there is a delay in the accumulation of full-length *nblA* mRNA upon nitrogen removal, and this delay is dependent on the presence of *as_nblA*. Via the TI mechanism, the asRNA establishes a nearly perfectly tight threshold linear response [63], which is difficult to achieve by mechanisms that require RNA–RNA interaction. This mechanism establishes a threshold response, such that *nblA* transcripts accumulate only when transcriptional activation exceeds a critical level. Furthermore, by incorporating previous data on NsrR1 in the model [10, 26], we conclude that NsrR1 also plays a crucial role in controlling *nblA* mRNA amount (Fig. 5C). Together, *as_nblA* and NsrR1 (to a lower extent) fully repress *nblA* synthesis in the presence of combined nitrogen (Fig. 5C), which explains the strong phenotype of Δ*as_nblA* observed in this work and the weaker phenotype of ΔNsrR1 strains [10] in this condition. In addition, this regulatory architecture also supports cell-type specificity within filaments. The model shows that the system allows that a roughly 3-fold synthesis rate difference between vegetative cells and heterocysts is amplified to a >11-fold change in the maximal *nblA* RNA accumulation (Fig. 5C). By introducing nonlinearity into the response, antisense transcription amplifies relatively small differences in transcriptional activity, contributing to the pronounced accumulation of NblA in heterocysts compared to vegetative cells. That allows a binary situation with high concentrations of NblA in heterocysts and low concentrations in vegetative cells as observed in *Tolypothrix* sp. [55].

In summary, the regulatory system we describe here operates by the transcription of an asRNA along with a *trans*-acting sRNA (Fig. 6). The double regulation of *nblA* ex-

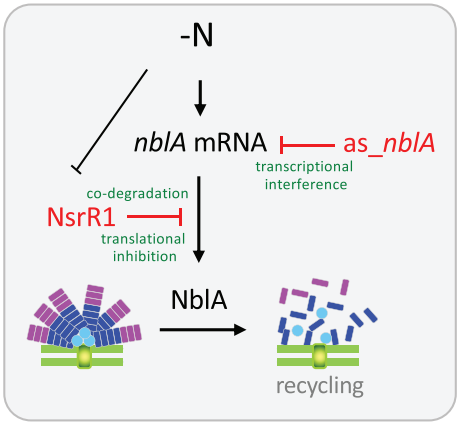

Figure 6. Model of the post-transcriptional regulation of NblA accumulation. The *nblA* mRNA is subjected to a double regulation operated by NsrR1, a sRNA that represses translation of the *nblA* mRNA [10] and co-degrades with the mRNA and *as_nblA*, an asRNA that inhibits accumulation of the *nblA* mRNA in the presence of ammonium by a TI mechanism. However, upon removal of combined nitrogen, NtcA activates transcription of *nblA*, overcoming TI by *as_nblA*, and represses transcription of *nsrR1*, resulting in the accumulation of *nblA* mRNA, leading to the production of NblA and PBS degradation.

pression by *as_nblA* and NsrR1 highlights the importance of additional regulatory elements that contribute to the suppression of background expression from transcriptionally regulated genes that, under non-inducing conditions, may be expressed due to leaky regulation of the promoter or, as in the case of *nblA*, because of readthrough upstream transcription. The regulatory mechanism operated by *as_nblA* seems conserved in heterocyst-forming cyanobacteria since the analysis of available transcriptomic data for *N. punctiforme* or *Nodularia* shows that also in these cyanobacteria there is a non-coding antisense transcript to *nblA* like *as_nblA* analyzed in this work (Supplementary Fig. S1). Interestingly, available data indicate that the accumulation of *nblA* and as_*nblA* exhibits opposite dynamics in response to light availability (Fig. 1 and Supplementary Fig. S1). Such inverse dynamics in the expression of two overlapping transcripts produced in opposite orientation (the so called excludon arrangement) has been observed in several bacteria [58]. Furthermore, in the unicellular strain *Synechocystis* sp. PCC 6803 (Supplementary Fig. S10), there is also antisense transcription to *nblA*, produced by overlapping transcription of an mRNA corresponding to a gene located downstream of *nblA* and transcribed in the opposite orientation [64, 65].

In conclusion, *nblA* expression is controlled by a multilayered regulatory system in which antisense transcription and a *trans*-acting sRNA cooperate to suppress basal expression and establish a threshold for induction. This combination enables precise control of a protein whose activity is beneficial under stress but deleterious when misregulated, illustrating the broader importance of antisense-mediated mechanisms in fine-tuning bacterial gene expression.

Acknowledgements

We are grateful to Professor Wolfgang R. Hess (University of Freiburg) for sharing the raw data used to elaborate Supplementary Fig. S10 and Alicia Orea (IBVF, CSIC-Universidad de Sevilla) for help with microscopy.

Author contributions: Isidro Álvarez-Escribano (Investigation, Visualization, Writing – review & editing), Manuel Brenes-Álvarez (Investigation, Visualization, Writing – review & editing), Jens Georg (Formal analysis, Methodology, Software, Visualization, Funding acquisition, Writing – review & editing), Agustín Vioque (Conceptualization, Investigation, Visualization, Writing – review & editing), and Alicia M. Muro-Pastor (Conceptualization, Funding acquisition, Investigation, Project administration, Visualization, Writing – original draft, Writing – review & editing)

Supplementary data

Supplementary data is available at NAR online.

Conflict of interest

None declared.

Funding

This work was supported by Agencia Estatal de Investigación, Spain (MCIN/AEI/10.13039/501100011033, FEDER, UE) (PID2019-105526GB-I00, PID2022-138128NB-I00 to A.M.M.-P.), and Deutsche Forschungsgemeinschaft (530000184 to J.G.). Funding to pay the Open Access publication charges for this article was provided by Consejo Superior de Investigaciones Científicas (CSIC), Spain.

Data availability

Raw RNA-seq data can be accessed in the GEO database under accession number GSE299220. The fitted model R object and the scripts are available at GitHub (https://github.com/JensGeorg/Bayesian-modeling-of-nblA-regulation.git) and Zenodo (https://doi.org/10.5281/zenodo.19221631).

References

1. Collier JL, Grossman AR. A small polypeptide triggers complete degradation of light-harvesting PBP in nutrient-deprived cyanobacteria. *Embo J* 1994;13:1039–47. https://doi.org/10.1002/j.1460-2075.1994.tb06352.x
2. Kato H, Kubo T, Hayashi M *et al.* Interactions between histidine kinase NblS and the response regulators RpaB and SrrA are involved in the bleaching process of the cyanobacterium *Synechococcus elongatus* PCC 7942. *Plant Cell Physiol* 2011;52:2115–22. https://doi.org/10.1093/pcp/pcr140
3. Bienert R, Baier K, Volkmer R *et al.* Crystal structure of NblA from *Anabaena* sp. PCC 7120, a small protein playing a key role in phycobilisome degradation. *J Biol Chem* 2006;281:5216–23. https://doi.org/10.1074/jbc.M507243200
4. Karradt A, Sobanski J, Mattow J *et al.* NblA, a key protein of phycobilisome degradation, interacts with ClpC, a HSP100 chaperone partner of a cyanobacterial Clp protease. *J Biol Chem* 2008;283:32394–403. https://doi.org/10.1074/jbc.M805823200
5. Nguyen AY, Bricker WP, Zhang H *et al.* The proteolysis adaptor, NblA, binds to the N-terminus of beta-phycocyanin: implications for the mechanism of phycobilisome degradation. *Photosynth Res* 2017;132:95–106. https://doi.org/10.1007/s11120-016-0334-y
6. Sendersky E, Kozer N, Levi M *et al.* The proteolysis adaptor, NblA, initiates protein pigment degradation by interacting with the cyanobacterial light-harvesting complexes. *Plant J* 2014;79:118–26. https://doi.org/10.1111/tpj.12543

7. Nadel O, Hanna R, Rozenberg A *et al.* Viral NblA proteins negatively affect oceanic cyanobacterial photosynthesis. *Nature* 2025;648:434–42. https://doi.org/10.1038/s41586-025-09656-x
8. Baier K, Lehmann H, Stephan DP *et al.* NblA is essential for phycobilisome degradation in *Anabaena* sp. strain PCC 7120 but not for development of functional heterocysts. *Microbiology* 2004;150:2739–49. https://doi.org/10.1099/mic.0.27153-0
9. Mitschke J, Vioque A, Haas F *et al.* Dynamics of transcriptional start site selection during nitrogen stress-induced cell differentiation in *Anabaena* sp. PCC7120. *Proc Natl Acad Sci USA* 2011;108:20130–5. https://doi.org/10.1073/pnas.1112724108
10. Álvarez-Escribano I, Vioque A, Muro-Pastor AM. NsrR1, a nitrogen stress-repressed sRNA, contributes to the regulation of *nblA* in *Nostoc* sp. PCC 7120. *Front Microbiol* 2018;9:2267. https://doi.org/10.3389/fmicb.2018.02267
11. Riediger M, Kadowaki T, Nagayama R *et al.* Biocomputational analyses and experimental validation identify the regulon controlled by the redox-responsive transcription factor RpaB. *iScience* 2019;15:316–31. https://doi.org/10.1016/j.isci.2019.04.033
12. Georg J, Hess WR. Widespread antisense transcription in prokaryotes. *Microbiol Spectr* 2018;6. https://doi.org/10.1128/microbiolspec.RWR-0029-2018
13. Flaherty BL, Van Nieuwerburgh F, Head SR *et al.* Directional RNA deep sequencing sheds new light on the transcriptional response of *Anabaena* sp. strain PCC 7120 to combined-nitrogen deprivation. *BMC Genomics* 2011;12:332. https://doi.org/10.1186/1471-2164-12-332
14. Brenes-Álvarez M, Vioque A, Muro-Pastor AM. Nitrogen-regulated antisense transcription in the adaptation to nitrogen deficiency in *Nostoc* sp. PCC 7120. *PNAS Nexus* 2023;2:pgad187. https://doi.org/10.1093/pnasnexus/pgad187
15. Olmedo-Verd E, Brenes-Álvarez M, Vioque A *et al.* A heterocyst-specific antisense RNA contributes to metabolic reprogramming in *Nostoc* sp. PCC 7120. *Plant Cell Physiol* 2019;60:1646–55. https://doi.org/10.1093/pcp/pcz087
16. Álvarez-Escribano I, Suárez-Murillo B, Brenes-Álvarez M *et al.* Antisense RNA regulates glutamine synthetase in a heterocyst-forming cyanobacterium. *Plant Physiol* 2024;195:2911–20. https://doi.org/10.1093/plphys/kiae263
17. Georg J, Hess WR. *cis*-Antisense RNA, another level of gene regulation in bacteria. *Microbiol Mol Biol Rev* 2011;75:286–300. https://doi.org/10.1128/MMBR.00032-10
18. Gatewood ML, Bralley P, Weil MR *et al.* RNA-seq and RNA immunoprecipitation analyses of the transcriptome of *Streptomyces coelicolor* identify substrates for RNase III. *J Bacteriol* 2012;194:2228–37. https://doi.org/10.1128/JB.06541-11
19. Lasa I, Toledo-Arana A, Dobin A *et al.* Genome-wide antisense transcription drives mRNA processing in bacteria. *Proc Natl Acad Sci USA* 2011;108:20172–7. https://doi.org/10.1073/pnas.1113521108
20. Lybecker M, Zimmermann B, Bilusic I *et al.* The double-stranded transcriptome of *Escherichia coli*. *Proc Natl Acad Sci USA* 2014;111:3134–9. https://doi.org/10.1073/pnas.1315974111
21. Callen BP, Shearwin KE, Egan JB. Transcriptional interference between convergent promoters caused by elongation over the promoter. *Mol Cell* 2004;14:647–56. https://doi.org/10.1016/j.molcel.2004.05.010
22. Chatterjee A, Johnson CM, Shu C-C *et al.* Convergent transcription confers a bistable switch in *Enterococcus faecalis* conjugation. *Proc Natl Acad Sci USA* 2011;108:9721–6. https://doi.org/10.1073/pnas.1101569108
23. Wanney WC, Youssar L, Kostova G *et al.* Improved RNA stability estimation indicates that transcriptional interference is frequent in diverse bacteria. *Commun Biol* 2023;6:732. https://doi.org/10.1038/s42003-023-05097-2
24. Rippka R, Deruelles J, Waterbury JB *et al.* Generic assignments, strain histories and properties of pure cultures of cyanobacteria. *Microbiology* 1979;111:1–61. https://doi.org/10.1099/00221287-111-1-1
25. Sambrook JF, Russell DW. Molecular cloning: a laboratory manual. Cold Spring Harbor, N Y: Cold Spring Harbor Laboratory, 2001.
26. Brenes-Álvarez M, Mitschke J, Olmedo-Verd E *et al.* Elements of the heterocyst-specific transcriptome unravelled by co-expression analysis in *Nostoc* sp. PCC 7120. *Environ Microbiol* 2019;21:2544–58. https://doi.org/10.1111/1462-2920.14647
27. Elhai J, Wolk CP. Conjugal transfer of DNA to cyanobacteria. *Methods Enzymol* 1988;167:747–54. https://doi.org/10.1016/0076-6879(88)67086-8
28. Merino-Puerto V, Mariscal V, Mullineaux CW *et al.* Fra proteins influencing filament integrity, diazotrophy and localization of septal protein SepJ in the heterocyst-forming cyanobacterium *Anabaena* sp. *Mol Microbiol* 2010;75:1159–70. https://doi.org/10.1111/j.1365-2958.2009.07031.x
29. Cai Y, Wolk CP. Use of a conditionally lethal gene in *Anabaena* sp. strain PCC 7120 to select for double recombinants and to entrap insertion sequences. *J Bacteriol* 1990;172:3138–45. https://doi.org/10.1128/jb.172.6.3138-3145.1990
30. Mohamed A, Jansson C. Influence of light on accumulation of photosynthesis-specific transcripts in the cyanobacterium *Synechocystis* 6803. *Plant Mol Biol* 1989;13:693–700. https://doi.org/10.1007/BF00016024
31. Brenes-Álvarez M, Olmedo-Verd E, Vioque A *et al.* Identification of conserved and potentially regulatory small RNAs in heterocystous cyanobacteria. *Front Microbiol* 2016;7:48. https://doi.org/10.3389/fmicb.2016.00048
32. Muro-Pastor AM, Valladares A, Flores E *et al.* The *hetC* gene is a direct target of the NtcA transcriptional regulator in cyanobacterial heterocyst development. *J Bacteriol* 1999;181:6664–9. https://doi.org/10.1128/JB.181.21.6664-6669.1999
33. Steglich C, Futschik ME, Lindell D *et al.* The challenge of regulation in a minimal photoautotroph: non-coding RNAs in *Prochlorococcus*. *PLoS Genet* 2008;4:e1000173. https://doi.org/10.1371/journal.pgen.1000173
34. Vioque A. Analysis of the gene encoding the RNA subunit of ribonuclease P from cyanobacteria. *Nucleic Acids Res* 1992;20:6331–7. https://doi.org/10.1093/nar/20.23.6331
35. Ionescu D, Voβ B, Oren A *et al.* Heterocyst-specific transcription of NsiR1, a non-coding RNA encoded in a tandem array of direct repeats in cyanobacteria. *J Mol Biol* 2010;398:177–88. https://doi.org/10.1016/j.jmb.2010.03.010
36. Riediger M, Spät P, Bilger R *et al.* Analysis of a photosynthetic cyanobacterium rich in internal membrane systems via gradient profiling by sequencing (Grad-seq). *Plant Cell* 2021;33:248–69. https://doi.org/10.1093/plcell/koaa017
37. Gonzalez A, Riley KW, Harwood TV. *et al.* A tripartite, hierarchical sigma factor cascade promotes hormogonium development in the filamentous cyanobacterium *Nostoc punctiforme*. *mSphere* 2019;4:e00231–19. https://doi.org/10.1128/mSphere.00231-19
38. Harwood TV, Risser DD. The primary transcriptome of hormogonia from a filamentous cyanobacterium defined by cappable-seq. *Microbiology* 2021;167:001111. https://doi.org/10.1099/mic.0.001111
39. Teikari JE, Hou S, Wahlsten M *et al.* Comparative genomics of the Baltic Sea toxic cyanobacteria *Nodularia spumigena* UHCC 0039 and its response to varying salinity. *Front Microbiol* 2018;9:356. https://doi.org/10.3389/fmicb.2018.00356
40. Kopf M, Möke F, Bauwe H *et al.* Expression profiling of the bloom-forming cyanobacterium *Nodularia* CCY9414 under light and oxidative stress conditions. *ISME J* 2015;9:2139–52. https://doi.org/10.1038/ismej.2015.16
41. Kim D, Paggi JM, Park C *et al.* Graph-based genome alignment and genotyping with HISAT2 and HISAT-genotype. *Nat Biotechnol* 2019;37:907–15. https://doi.org/10.1038/s41587-019-0201-4

42. Li H. Aligning sequence reads, clone sequences and assembly contigs with BWA-MEM. *arXiv*, https://doi.org/10.48550/arXiv.1303.3997, 16 Mar 2013, preprint; not peer reviewed.
43. Li H, Handsaker B, Wysoker A *et al.* The sequence alignment/map format and SAMtools. *Bioinformatics* 2009;25:2078–9. https://doi.org/10.1093/bioinformatics/btp352
44. Liao Y, Smyth GK, Shi W. featureCounts: an efficient general purpose program for assigning sequence reads to genomic features. *Bioinformatics* 2014;30:923–30. https://doi.org/10.1093/bioinformatics/btt656
45. Love MI, Huber W, Anders S. Moderated estimation of fold change and dispersion for RNA-seq data with DESeq2. *Genome Biol* 2014;15:550. https://doi.org/10.1186/s13059-014-0550-8
46. Segel LA, Slemrod M. The quasi-steady-state assumption: a case study in perturbation. *SIAM Rev* 1989;31:446–77. https://doi.org/10.1137/1031091
47. Shearwin KE, Callen BP, Egan JB. Transcriptional interference—a crash course. *Trends Genet* 2005;21:339–45. https://doi.org/10.1016/j.tig.2005.04.009
48. Sneppen K, Dodd IB, Shearwin KE *et al.* A mathematical model for transcriptional interference by RNA polymerase traffic in *Escherichia coli*. *J Mol Biol* 2005;346:399–409. https://doi.org/10.1016/j.jmb.2004.11.075
49. Carpenter B, Gelman A, Hoffman MD *et al.* Stan: a probabilistic programming language. *J Stat Soft* 2017;76:1–32. https://doi.org/10.18637/jss.v076.i01
50. Gabry J, Češnovar R, Johnson A. cmdstanr: r interface to 'CmdStan'_. R package version 0.7.1. 2024.
51. Muro-Pastor AM. The heterocyst-specific NsiR1 small RNA is an early marker of cell differentiation in cyanobacterial filaments. *mBio* 2014;5:e01079–14. https://doi.org/10.1128/mBio.01079-14
52. Schindelin J, Arganda-Carreras I, Frise E *et al.* Fiji: an open-source platform for biological-image analysis. *Nat Methods* 2012;9:676–82. https://doi.org/10.1038/nmeth.2019
53. Lowry OH, Rosebrough NJ, Farr AL *et al.* Protein measurement with the Folin phenol reagent. *J Biol Chem* 1951;193:265–75. https://doi.org/10.1016/S0021-9258(19)52451-6
54. Chen H, Shiroguchi K, Ge H *et al.* Genome-wide study of mRNA degradation and transcript elongation in *Escherichia col i*. *Mol Syst Biol* 2015;11:781. https://doi.org/10.15252/msb.20145794
55. Ochoa de Alda JAG, Lichtlé C, Thomas JC *et al.* Immunolocalization of NblA, a protein involved in phycobilisome turnover, during heterocyst differentiation in cyanobacteria. *Microbiology* 2004;150:1377–84. https://doi.org/10.1099/mic.0.26992-0
56. Kaneko T, Nakamura Y, Wolk CP *et al.* Complete genomic sequence of the filamentous nitrogen-fixing cyanobacterium *Anabaena* sp. strain PCC 7120. *DNA Res* 2001;8:205–13; https://doi.org/10.1093/dnares/8.5.205
57. O'Connor NJ, Bordoy AE, Chatterjee A. Engineering transcriptional interference through RNA polymerase processivity control. *ACS Synth Biol* 2021;10:737–48. https://doi.org/10.1021/acssynbio.0c00534
58. Sanmartín Á, Iturbe P, Rodríguez-Beltrán J *et al.* ExcludonFinder: mapping transcriptional overlaps between neighboring genes. *Nucleic Acids Res* 2025;53:gkaf686. https://doi.org/10.1093/nar/gkaf686
59. Sesto N, Wurtzel O, Archambaud C *et al.* The excludon: a new concept in bacterial antisense RNA-mediated gene regulation. *Nat Rev Microbiol* 2013;11:75–82. https://doi.org/10.1038/nrmicro2934
60. Fischer M, Hoffmann S. Transcriptional interference revisited. *Nat Genet* 2026;58:974–83. https://doi.org/10.1038/s41588-026-02536-8
61. Sudzinová P, Knežová Balgová T, Schwarz M *et al.* Bacteria sense the antibiotic rifampicin through a widespread dual-promoter based alarm system. *Nucleic Acids Res* 2026;54:gkaf1407. https://doi.org/10.1093/nar/gkaf1407
62. Hoffmann SA, Hao N, Shearwin KE *et al.* Characterizing transcriptional interference between converging genes in bacteria. *ACS Synth Biol* 2019;8:466–73. https://doi.org/10.1021/acssynbio.8b00477
63. Levine E, Hwa T. Small RNAs establish gene expression thresholds. *Curr Opin Microbiol* 2008;11:574–9. https://doi.org/10.1016/j.mib.2008.09.016
64. Kopf M, Klähn S, Pade N *et al.* Comparative genome analysis of the closely related *Synechocystis* strains PCC 6714 and PCC 6803. *DNA Res* 2014;21:255–66. https://doi.org/10.1093/dnares/dst055
65. Kopf M, Klähn S, Scholz I *et al.* Comparative analysis of the primary transcriptome of *Synechocystis* sp. PCC 6803. *DNA Res* 2014;21:527–39. https://doi.org/10.1093/dnares/dsu018

Received: March 27, 2026. **Revised:** May 12, 2026. **Accepted:** May 21, 2026